Kinetic Analysis of High Affinity Forms of Interleukin (IL)-13 Receptors: Suppression of IL-13 Binding by IL-2 Receptor γ Chain

Vladimir A. Kuznetsov*# and Raj K. Puri*

*Laboratory of Molecular Tumor Biology, Division of Cellular and Gene Therapies, Center for Biologics Evaluation and Research, FDA, Bethesda, Maryland 20892 and #Laboratory of Mathematical ImmunoBiophysics, Institute of Biochemical Physics of the Russian Academy of Sciences, Kosygin Str. 4/8, Moscow 117977, Russia

ABSTRACT Interleukin-13 (IL-13) is a pleiotropic cytokine that controls growth, differentiation, and apoptosis of immune and tumor cells. To understand the mechanisms of interaction between IL-13 and IL-13 receptors (IL-13R), and the role of the IL-2 receptor common γ chain (γ_c) in IL-13 binding and processing, we have examined IL-13 binding kinetics, dissociation/shedding, and internalization in renal cell carcinoma (RCC) cell lines. We observed a new phenomena in that the apparent rate of association, but not the dissociation, was strongly related to IL-13 concentration. We also observed cooperativity phenomena in IL-13 and IL-13R interaction in control RCC (ML_{neo}) cells, but not in cells transfected with γ_c chain (ML_{γ_c}). The number of IL-13 binding sites, the effective rate of ligand association, and the dissociation rate constants were reduced in γ_c-transfected cells compared to control RCC cells. Two forms of IL-13R were detected in these cell lines, which differed in the kinetics of endocytosis and dissociation/exocytosis. Only a small fraction of bound receptors (14–24%) was rapidly internalized and the same fraction of the ligand-receptor complexes was shed and/or dissociated. The expression of γ_c chain did not change any of these processes. A two independent high-affinity and moderate-affinity receptor model fit the kinetic observations in γ_c-transfected cells. However, in control cells, the binding kinetics were more complicated. A mathematical model that fit a set of kinetic and steady state data in control cells was selected from a set of possible models. This best-fit model predicts that 1) two different IL-13R are expressed on the cell membrane, 2) a minor fraction of IL-13R exist as microclusters (homodimers and/or heterodimers) without exogenous IL-13, 3) high morphological complexity of the γ_c-negative control cell membrane affects the cooperativity phenomena of IL-13 binding, and 4) a large number of co-receptor molecules is present, which helps keep the ligand on the cell surface for a long period of time after fast IL-13 binding and provides a negative control for ligand binding via production of the high affinity inhibitor bound to IL-13. Our data demonstrate that γ_c exerts dramatic changes in the kinetic mechanisms of IL-13 binding.

INTRODUCTION

Human interleukin (IL)-13 is a 12-kDa pleiotropic cytokine that is expressed in activated Th1 and Th2 lymphocytes (Minty et al., 1993; McKenzie et al., 1993), stimulated keratinocytes, activated mast cells and transformed B lymphocytes (Minty et al., 1993; McKenzie et al., 1993; de Waal, 1993). It inhibits proliferative activity of normal B cells and their precursors, B-CLL cells, and it protects B-CLL cells from spontaneous apoptosis (Chaouchi et al., 1996). A number of biological effects recently reported for IL-13 were previously observed for IL-4. But, in contrast to IL-4, IL-13 has not been shown to modulate growth characteristics of T lymphocytes (Zurawski and de Vries, 1994).

The effects of IL-13 are mediated by specific plasma membrane receptors (R). We have recently reported that a variety of human solid tumor cells express intermediate to high affinity IL-13R* and that their interaction with IL-13 inhibits growth of some human RCC cells (Obiri et al. 1996a). We proposed that IL-13R exists in three or four different forms in various cell types (Obiri et al., 1997). Type *I* IL-13R expressed in human RCC cells appear to be composed of a homodimer of p65-70 proteins [termed IL-13Rα_1 (or α') and α_2 (or α)]. In type *II* IL-13R, IL-13Rα_1 forms a heterodimer with IL-4R p140 chain termed IL-4Rβ. In types *III* and *IV* IL-13R, IL-13 binds IL-13Rα_1 and IL-4Rβ subunits and IL-2Rγ-chain (γ_c) may (type *III*) or may not (type *IV*) modulate IL-13 binding (Obiri et al., 1996b).

Although, the structure and biological properties of IL-13R are being vigorously investigated, the kinetics of IL-13 binding, dissociation, internalization, shedding, recycling, and degradation have not been studied. Knowledge of the biophysical and biochemical mechanisms of these processes is necessary for an understanding of the mechanisms of intracellular signaling and biological response of target cells. Fitting mathematical models that correspond to the kinetics of these processes may result in better understanding of the biochemical and biophysical properties of IL-13R, similar to IL-2R, IL-4R (Goldstein et al., 1992; Kuznetsov and Borisova, 1995a; Borisova and Kuznetsov, 1996) and other receptor systems (Gex-Fabry and DeLisi, 1984; Bajzer et al., 1989; Wofsy et al., 1992; Rovati et al.,

Received for publication 23 September 1997 and in final form 6 April 1999.

Address reprint requests to Dr. Raj K. Puri, Laboratory of Molecular Tumor Biology, Division of Cellular and Gene Therapies, Center for Biologics Evaluation and Research, FDA, NIH Building 29B, Room 2NN10, 29 Lincoln Drive, MSC 4555, Bethesda, MD 20892.

Dr. Kuznetsov's current address is Civilized Software, Inc., 8120 Woodmont Ave. 250, Bethesda, MD 20814. Tel: 301-652-4714; Fax: 301-656-1069; e-mail: cis@civilized.com.

*Abbreviations used: IL-13R, IL-13 receptor; ^{125}I-IL-13, ^{125}I-labeled interleukin-13; rhIL-13, recombinant human IL-13; RCC, renal cell carcinoma.

0006-3495/99/07/154/19 $2.00

1996). In this manuscript, we have studied IL-13 binding kinetics on two RCC cell lines (HL-RCC and ML-RCC) and evaluated the influence of γ_c gene expression on IL-13 and IL-13R interaction in ML-RCC cells transfected with γ_c cDNA. The kinetics of binding, dissociation, shedding of IL-13R, and ligand-induced receptor-mediated endocytosis of ligand has been investigated. We used mathematical models to analyze the kinetics of IL-13 binding to its receptors.

MATERIALS AND METHODS

Cytokines and reagents

Recombinant human IL-13 was expressed in *Escherichia coli* and purified as described (Debinski et al., 1995).

Cells

The RCC cell lines ML-RCC and HL-RCC were established in our laboratory from primary surgical tissues and were maintained in HEPES buffered DMEM with high glucose supplemented with glutamine plus 10% fetal bovine serum (FBS) and antibiotics (penicillin, 100 U/mL and streptomycin, 100 μg/mL) (Obiri et al., 1993). The γ_c-cDNA, along with neomycin transferase cDNA, was transfected into ML-RCC cells as previously described (Puri et al., 1996b).

Iodination of IL-13

IL-13 was labeled with ^{125}I (Amersham Research Products, Arlington Heights, IL) using IODO-GEN reagent (Pierce, Rockford, IL) according to the manufacturer's instructions. The specific activity of the radiolabeled IL-13 was estimated to range from 80 to 120 μCi/μg protein (Obiri et al., 1995).

Kinetics of IL-13 binding and dissociation

All binding and dissociation experiments were performed at 4°C to prevent receptor-mediated IL-13 internalization. The association kinetic studies were performed by incubating 0.5×10^6 or 1.0×10^6 cells with various concentrations (10–500 pM) of ^{125}I-IL-13 in 120 μL binding buffer (RPMI 1640 containing 0.2% human serum albumin and 10 mM HEPES) for 3 min to 18 h at 4°C. Nonspecific binding was determined for each ^{125}I-IL-13 concentration and each time point by co-incubation with 50 nM unlabeled IL-13. In some cases, nonspecific binding was established by determining total ^{125}I-IL-13 bound to cells after a short incubation (3–6 min) with radio-labeled IL-13. Both techniques gave similar results and the average value of these data was used as the nonspecific binding. The specific fraction of bound ligand was calculated by

$$z(t_i)/y_0 = \frac{\mathrm{cpm_i} - \mathrm{cpm_n}}{\mathrm{cpm_{tot}} - \mathrm{cpm_n}}, \quad (1)$$

where y_0, and z are the initial concentration of the radio-labeled ligand in the medium and the concentration of specifically bound ligand at time t_i, respectively; $z(t_i)/y_0$ is the specific bound fraction of ^{125}I-IL-13 at time t_i, $i = 1, 2, 3, \ldots$, and $\mathrm{cpm_i}$, $\mathrm{cpm_{tot}}$, $\mathrm{cpm_n}$ represent cpm for bound, total, and nonspecifically bound ^{125}I-IL-13.

Cell-bound ^{125}I-IL-13 was separated from unbound ligand by centrifugation through a cushion of phthalate oils (Obiri et al., 1995). Radioactivity in the cell pellets and supernatants was counted in a gamma-counter.

For dissociation kinetic assays, aliquots were taken after 4–6 h of incubation at 4°C, which allowed time to attain a state of equilibrium at the concentration of ligand used. Cells were then centrifuged at $1500 \times g$ for 5 min to remove free radioactive material, washed twice with cold PBS and resuspended to the initial volume with binding buffer containing 50 nM unlabeled IL-13. At different time intervals, bound and free ligand was measured as described above.

Competitive binding assays at 4°C

Two types of competitive binding experiments were performed. In the first set of experiments, the binding of a single concentration of labeled IL-13 in the presence of various concentrations of unlabeled IL-13 (from 0 to 200 nM) at 4°C was measured at fixed time points. In the second set of experiments, the binding of various concentrations of labeled IL-13 and a single concentration of unlabeled ligand was determined at various times from 2 min to 14 h.

Internalization assay

The γ_c negative control ($\mathrm{ML_{neo}}$) or γ_c transfected ($\mathrm{ML}\gamma_c$) RCC cells or HL-RCC cells were incubated in binding buffer containing 0.2 nM chloroquine at 37°C for 5 min to prevent degradation of internalized IL-13 (Obiri and Puri, 1994). Cells were then washed and 2.5×10^6 cells of each type were incubated with 0.2 or 0.3 nM ^{125}I-IL-13 at 4°C for 4.5 h, after which unbound ligand was washed away with PBS. The cell pellets were suspended in binding buffer and then quickly brought to 37°C. At various time intervals, two duplicate sets of 50 μL aliquots were taken. One set was incubated with 100 μL glycine buffer (25 mM glycine, 125 mM NaCl, final pH = 2.0) at 4°C for 10 min. The suspension was then centrifuged through a mixture of phthalate oils and the radioactivity in the cell pellet (acid resistant or internalized (C_{in}) and in the supernatant (surface bound + dissociated, $C_s + C_{out}$) was measured with a gamma counter. The other set of 50 μL aliquots was directly centrifuged through phthalate oils and the radioactivity measured in the supernatant was used for dissociated ^{125}I-IL-13 values (C_{out}). Surface bound ^{125}I-IL-13 was determined by subtracting internalized ^{125}I-IL-13 values from surface bound + internalized values. Internalized, dissociated, and surface bound radioactivity values were added to obtain total bound value cpm.

Fractions of specific surface bound (C_s), internalized (C_{in}) and shed/dissociated (C_{out}) ligand were calculated by

$$C_s = a/(a + b) - (c - c_0)/(c + d),$$

$$C_{in} = (c - c_0)/(c + d),$$

$$C_{out} = b/(a + b),$$

where a = bound + internalized, b = dissociated ligand, c = internalized ligand, d = bound + dissociated ligand, $a + b$ is the total in experiment 1 (without glycine treatment); $c + d$ is the total in experiment 2 (after glycine treatment); c_0 is the nonspecific internalized ligand. The kinetic parameters for the internalization experiments were estimated by the two independent binding sites model (Kuznetsov, 1990).

Analysis of association kinetics by one binding site model

Kinetic binding of IL-13 was analyzed by one binding site model. According to this model,

$$x + y \underset{k_{-1}}{\overset{k_1}{\rightleftharpoons}} z, \quad (2)$$

where x, y, and z are the concentrations of unbound receptor, unbound ligand, and their bound pairs [$z = (x + y)$], respectively, and k_1, k_{-1} are the association and dissociation rate constants for reaction 2, respectively. For

fitting the model to kinetic data, we used the exact solution of the differential equation which corresponds to the kinetic scheme 2 as described by Kuznetsov (1996).

A fractal analysis of IL-13 binding kinetics

The model of diffusion of a ligand in homogeneous solution to a fractal dimension surface where it forms a ligand-receptor complex was described by Havlin (1989). For analysis of binding of macromolecules to membrane receptors, this model can be rewritten as

$$\frac{z(t)}{y_0} \simeq N_c R_0 k_1 \begin{cases} t^{(3-D_f)/2} & \text{at} \quad t < t_c \\ t^{1/2} & \text{at} \quad t > t_c, \end{cases} \tag{3}$$

where z is the concentrations of bound ligand-receptor pairs, y_0 is the initial concentration of the ligand in the medium far from the cell surface, N_c is the concentration of cells, and R_0 is the average number of receptor molecules per cell ($R_0 = x_0/N_c$), where x_0 is the initial concentration of receptor. k_1 is the binding rate of ligand to receptor, D_f is the fractal dimension (complexity) of the surface, t_c is the characteristic time when regular diffusion of ligand to the cell surface dominates. The effective binding rate by this model is $\kappa_f = k_1 R_0 N_c$. Eq. 3 indicates that, in the fractal kinetic reaction, the concentration of ligand-receptor complex on cell surfaces $z(t)$ is proportional to t^p, where $p = (3 - D_f)/2$ during the early reaction period ($t < t_c$), and $p = ½$ outside (Havlin, 1989).

Analysis of kinetic association data by a two independent binding site model

Our kinetic experiments were also analyzed using the kinetic scheme,

$$x_1 + y \underset{k_{-1}}{\overset{k_1}{\rightleftharpoons}} z_1, \qquad x_2 + y \underset{k_{-2}}{\overset{k_2}{\rightleftharpoons}} z_2, \tag{4}$$

where y, x_1, x_2 are the concentrations of the free ligand and their two forms of independent receptors, respectively, and z_1, z_2 are the concentrations of ligand-receptor pairs. The system of ordinary differential equation corresponding to this kinetic scheme was used to evaluate the rate constants of binding (k_1, k_2) and of dissociation (k_{-1}, k_{-2}) by curve-fitting.

Analysis of kinetic dissociation data

Dissociation data were analyzed using both the one receptor and two independent receptor models. For the first model, the fraction of bound ligand in time was described by

$$z(t)/z(\tau) = \exp(-k_{-1}t), \tag{5}$$

where t is time in the dissociation assay, τ is binding time, $t > \tau$; $z(\tau)$ is ligand bound to the receptor after binding time τ; and k_{-1} is the dissociation rate constant.

For the two independent receptor model, the time course of dissociation was described with the two-exponential equation,

$$\begin{aligned} B(t) &= z_{tot}(t)/z_{tot}(\tau) \\ &= (1 - d(\tau))\exp(-k_{-1}t) + d(\tau)\exp(-k_{-2}t), \end{aligned} \tag{6}$$

where z_{tot} is the sum concentration of the fast (z_1) and slow (z_2) receptors, which differed with the rate of ligand dissociation, t is the current time of dissociation, and τ is the time of IL-13 binding on the cells after which the dissociation experiment was started. $z_{tot}(t) = z_1(t) + z_2(t)$ is the concentration of ligand bound to the slow (z_1) and fast (z_2) species at time $t > \tau$, $d(\tau) = z_2(\tau)/z_{tot}(\tau)$. k_{-1}, k_{-2} are the dissociation rates observed for each species. Other parameters are the same as defined above.

Mathematical modeling for internalization kinetics

Two simple mathematical models for processing kinetics (Kuznetsov and Borisova, 1995a) were fit to the experimental data of the internalization assay. For the first model, we presumed that a single IL-13–IL-13R complex is formed and that it follows a single pathway for internalization, dissociation, and shedding. For the second model, we assumed that two independent IL-13–IL-13R complexes are formed, each of them having a separate pathway of processing after ligand binding. Both models assume that a concentration of unbound ligand is negligibly low. For the second model, the following differential equations were used:

$$\frac{dz_f(t)}{dt} = -(\kappa_1 + \kappa_{in})z_f, \qquad \frac{dz_s(t)}{dt} = -(\kappa_2 + \kappa'_{in})z_s, \tag{7}$$

$$\frac{dz_{in}(t)}{dt} = \kappa_{in} z_f + \kappa'_{in} z_s, \qquad \frac{dz_{out}(t)}{dt} = \kappa_1 z_f + \kappa_2 z_s,$$

where z_f, z_s are the type 1 and 2 ligand-receptor complex (LRCs) on the cell surface, and z_{in}, z_{out} are the internalized and shed/dissociated LRCs, respectively. Initial conditions (at $t_0 = \tau$) are defined as $z_f(\tau) = z_{f0}$, $z_s(\tau) = z_{s0}$, $z_{in}(\tau) = z_{out}(\tau) = 0$; κ_1, κ_2 are the constant rates for shedding/dissociation of the ligand/receptor type 1 complexes and ligand/receptor type 2 complexes, respectively. κ_{in}, κ'_{in} are the constant rates for internalization of the ligand/receptor type 1 complexes and ligand/receptor type 2 complexes, respectively. Five parameters, $f_0 (f_0 = z_{f_0}/(z_{f_0} + z_{s_0}))$, κ_i ($i = 1, 2$), κ_{in}, κ'_{in} were estimated by fitting the model, Eq. 7, to the internalization assay data by the method described in Kuznetsov (1990).

Proliferation assay

ML_{neo} and $ML\gamma_c$-transfected RCC cells were harvested, washed, and resuspended in culture medium and 3.5×10^4 cells were plated in 10-cm^2 tissue culture-treated Petri dishes (Falcon, Dickinson, Lakeridge, NJ) with culture medium and cultured for different periods of time at 37°C in a 5% CO_2 environment. After 52, 72, 96, 124, 144, and 240 h of incubation, a number of live cells was determined in duplicate dishes for each cell line by harvesting the cells with versene, washing them, and resuspending to 0.25–0.5 mL for direct cell counts using a hemacytometer.

Simulation procedure

Simulations based on the nonlinear ordinary differential equations (stiff method) corresponding to the models presented in this paper were performed using MLAB modeling system (Civilized Software, Inc.; www.civilized.com).

Procedures for fitting of nonlinear kinetic systems

For estimating parameters of the models, we used both the direct nonparametric weighted global optimization method (Kuznetsov et al., 1993) and the curve-fitting facilities of the MLAB mathematical and statistical modeling system (Knott, 1996). A goodness-of-fit analysis of the models was applied for data from association, dissociation, and displacement assays as separate sets of data and pooled together. To get more accurate and robust estimates of parameters, we used a cross-validation procedure for parameter estimation (V. A. Kuznetsov and G. D. Knott, in preparation). In this approach, each experimental curve, in turn, was eliminated from the fitting procedure. Then, the set of the best parameters was evaluated by fitting the other experimental curves, and these parameter estimates were used to calculate the sum of squared deviations of the predicted kinetic curve points from the excluded experimental points. The reciprocals of these sums were used as the weights of the set of evaluated parameters. Wil-

coxon two-sample signed-rank testing and the method of Durbin and Watson for testing the null hypothesis of serial independence of residuals in the least squares analysis against the existence of positive or negative correlation were applied.

RESULTS

Kinetic binding of ^{125}I-IL-13 and dissociation kinetics at 4°C

As shown in Fig. 1 *A,* the binding of radiolabeled IL-13 to control ML_{neo} γ_c-negative cells reached steady state after 1 h, and persisted for up to 10 h. Similar forms of this kinetic curve were observed when 50 nM unlabeled IL-13 was added in the reaction mixture (*open circles,* Fig. 1 *A*). The level of specific IL-13 binding was reduced in γ_c-transfected cells compared to control cells (Fig. 1 *B*). In addition, the apparent rate of binding in γ_c-transfected cells was slower compared to control cells. Furthermore, the steady-state level of binding was reached between 4 and 5.5 h of incubation, compared to 1 h in control ML_{neo} cells (Fig. 1 *B*). The fraction of bound ^{125}I-IL-13 to MI_γ RCC cells was much smaller than in control γ_c-negative cells (Fig. 1 *A* and *C*).

The rate of dissociation of a small fraction (10–20%) of bound ligand was rapid in the initial phase (up to 10–20 min), but this was followed by a very slow phase in all RCC cell lines (Fig. 1 *D, E,* and *F*). Such a slow dissociation rate is unusual for cytokine receptors: most of them have half-lives of 1–30 min. The calculated half-life, $t_{1/2}$, of the slow-dissociated ligand on HL, ML_{neo}, and ML_γ RCC cells

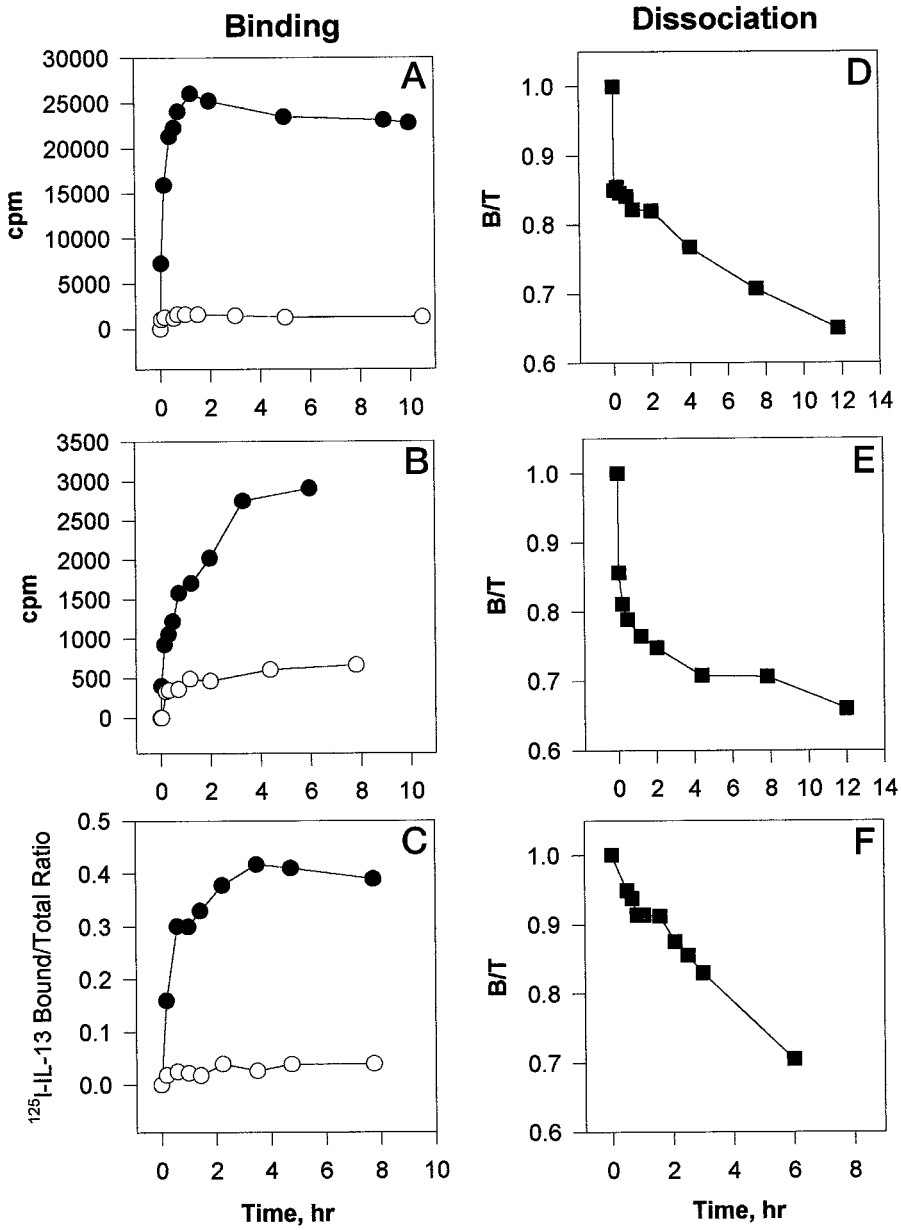

FIGURE 1 Time-dependent binding and dissociation of ^{125}I-IL-13 in RCC cells. 0.5×10^6 control ML_{neo} (*A*), γ_c-transfected RCC cells (*B*) were incubated with 200 pM ^{125}I-IL-13 and 1×10^6 HL-RCC cells (*C*) were incubated with 100 pM ^{125}I-IL-13 at 4°C with and without 50 nM of unlabeled IL-13 for indicated period of time. Cell-bound and free ligand were measured as described in Materials and Methods. *Black circles,* mean values of two determinations in a direct binding assay; *open circles,* mean values in a displacement binding assay. ML_{neo} 10^6 (*D*) and $ML\gamma_c$-transfected (*E*) RCC cells were incubated with 200 pM ^{125}I-IL-13 and 10^6 HL (*F*) RCC cells incubated with 300 pM for 5 h at 4°C, washed from unbound radiolabeled ligand and cells were used for dissociation assays. Unlabeled IL-13 100 pM was added immediately after washing the cells to prevent rebinding of radiolabeled ligand. Data for dissociation curves were corrected for nonspecific dissociation. The SDs for experimental points were not larger than the size of symbols presented on the figure. Association and dissociation assays were performed in the same session. Data for ML- and HL-RCC cell lines were obtained in separate experiments. By trypan blue staining, 85–90% cells were alive in binding buffer after 12 h incubation at 4°C. Experiments were repeated two times with similar results.

was 13.3 ± 1 h, 27 ± 3 h and 43 ± 4 h, (mean ± SD), respectively. These results indicate that IL-13 binding and dissociation at 4°C in γ_c-transfected RCC cells is slower than control cells.

Dissociation kinetics after binding of different concentrations of IL-13 at 4°C

To determine whether dissociation kinetics vary with different concentration of bound ^{125}I-IL-13, we measured the rate of dissociation after preincubation of ML-RCC cells with various concentrations of ^{125}I-IL-13 for 3.5–5 h. As shown in Fig. 2 *A–C,* in control ML_{neo} RCC cells, ^{125}I-IL-13 dissociation kinetics did not vary with different amounts of bound ^{125}I-IL-13. The effective rate of the slow phase of dissociation, k_{-1}, was 0.023 h^{-1}, 0.017 h^{-1}, 0.025 h^{-1}, and 0.027 h^{-1} at 15, 70, 200, and 500 pM of ^{125}I-IL-13, respectively. Similar results were obtained in γ_c-transfected cells (Fig. 2 *D–F*). The effective dissociation rates at 15, 150, 200, and 300 pM ^{125}I-IL-13 were 0.014 h^{-1}, 0.016 h^{-1}, 0.017 h^{-1}, and 0.018 h^{-1}, respectively. Thus, the rate of the slow phase of IL-13 dissociation from its receptor did not depend on the amount of bound ligand; however, transfection of γ_c chain reduced this rate by 1.6 times ($p < 0.05$).

^{125}I-IL-13 binding in the presence of different concentrations of ^{125}IL-13 at 4°C

It has been reported for several ligand-receptor systems that the effective binding rate varies with the concentration of ligand (Park et al., 1987; Sadana and Beelaram, 1996b; Franco et al., 1996). We, therefore, examined whether the association rate of ^{125}I-IL-13 varied with the ligand concentration. We performed these experiments using 10 to 500 pM ^{125}I-IL-13. Additionally, in some experiments, we used two concentrations of target cells, 0.5×10^6 and 1×10^6.

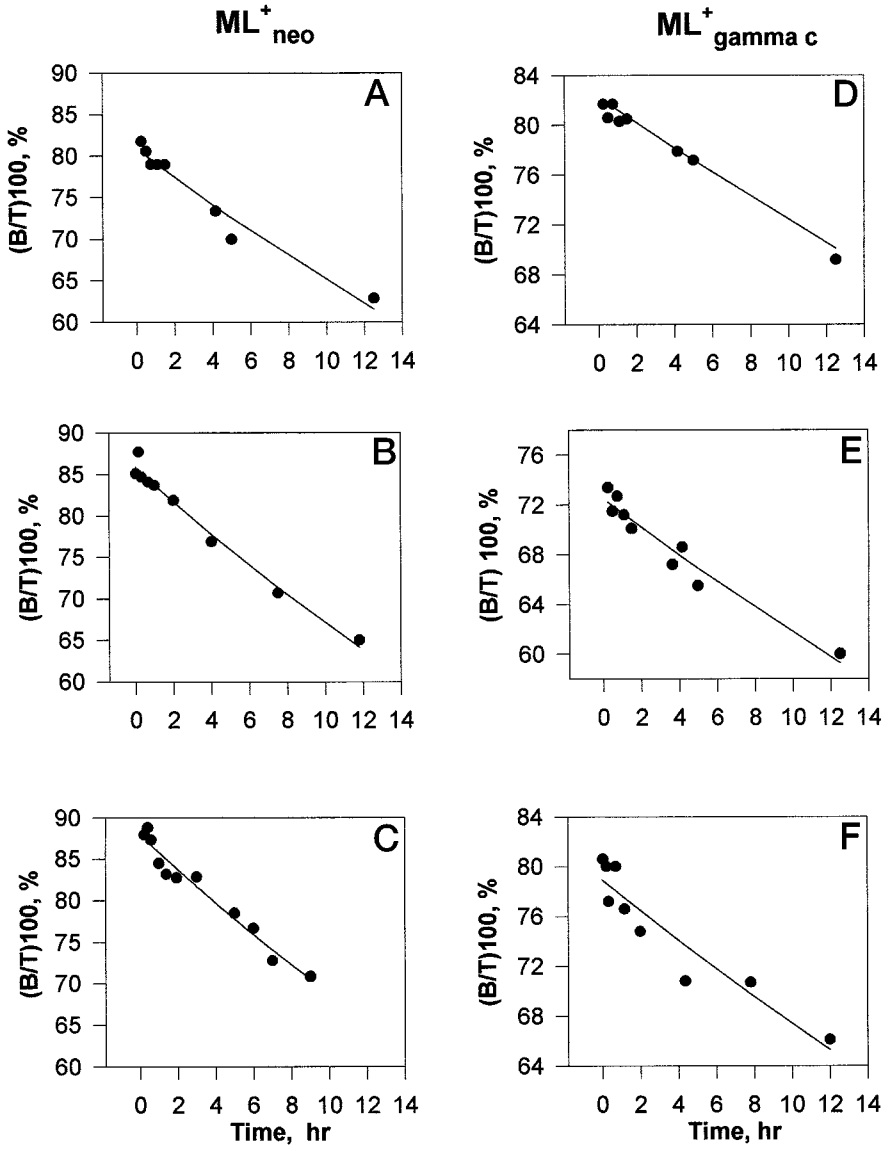

FIGURE 2 Dissociation kinetics of IL-13 from IL-13R on control and MLγ_c-RCC cells. Values represent the averages of duplicate determination. Time-dependence of ^{125}I-IL-13 dissociation at initial concentrations 15 pM (*A*, *D*), 150 pM (*B*, *F*) and 200 pM (*C*, *E*) were fitted by the one-exponential model (*solid curves*). The SD of mean values was not larger then 0.06. These experiments were repeated two times with similar results.

As shown in Fig. 3, *A* and *B*, the slope of the normalized binding curves increased monotonically with the ligand concentration in control ML_{neo} cells, but, in contrast, the slope decreased in γ_c-transfected cells. These results suggest that the binding rate and/or number of available binding sites in γ_c-negative RCC cells increase with the concentration of ligand, and γ_c-transfection suppresses the positive cooperative mechanism of binding of IL-13 to its receptor(s).

Sadana and Beelaram (1996b) successfully applied kinetic fractal models to interpret the dependence of binding rate constants on ligand concentration in biosensor systems. These models describe the effect of topological complexity (fractal dimension) of the surfaces that carry the specific receptor. Surface complexity imposes 1) heterogeneity in the rate of ligand binding due to the geometric difficulty of diffusion of ligand to different surface regions, and 2) a nonuniform distribution of receptor molecules on the surfaces. We show that this type of model can be also applied to the analysis of IL-13 binding on cell surfaces. Figure 3, *A* and *B* shows that Eq. 3 fits well to the initial (transit) phase of specific IL-13 binding data. The effective rate of IL-13 binding by the fractal kinetic model, κ_f ($\kappa_f = k_1 x_0$), increased from $0.41 \pm 0.01\ h^{-1}$ to a saturation level of $0.58 \pm 0.004\ h^{-1}$ in control ML_{neo} cells (Fig. 3 *C*), but it was very low ($\kappa_f = 0.029 \pm 0.007\ h^{-1}$) and independent of an initial concentration of IL-13 in the γ_c-transfected cells. This analysis shows that transfection of γ_c chain reduces the effective rate of binding, κ_f, by a factor of 20.

The D_f, parameter of Eq. 3, is the fractal dimension of the cell membrane that displays how much space it occupies. This parameter is a measure of the degree of complexity of the natural or artificial surfaces, and it also characterizes the degree of irregularity of the distribution of binding sites on the surface (Havlin, 1989; Sadana and Beelaram, 1996b). Figure 3 *D* shows that D_f increases with increasing concentrations of IL-13 at low initial concentrations of IL-13. However, at higher concentrations of ligand, this parameter did not change. The constant level of D_f in control cells was significantly higher than in γ_c-transfected RCC cells.

Thus, fractal kinetic analysis exhibits an anomalous reaction order and concentration dependence of the association rate coefficient in control γ_c-negative cell line; however, in γ_c-transfected cells, these effects were not observed.

Analysis of binding/dissociation kinetics by one receptor model

The effective rate of binding of IL-13, κ_f, is defined as a product of the association rate constant (k_1) and the number of binding sites R_0. The rapid effective rate observed in ML_{neo} cells, suggests a higher rate of binding or higher

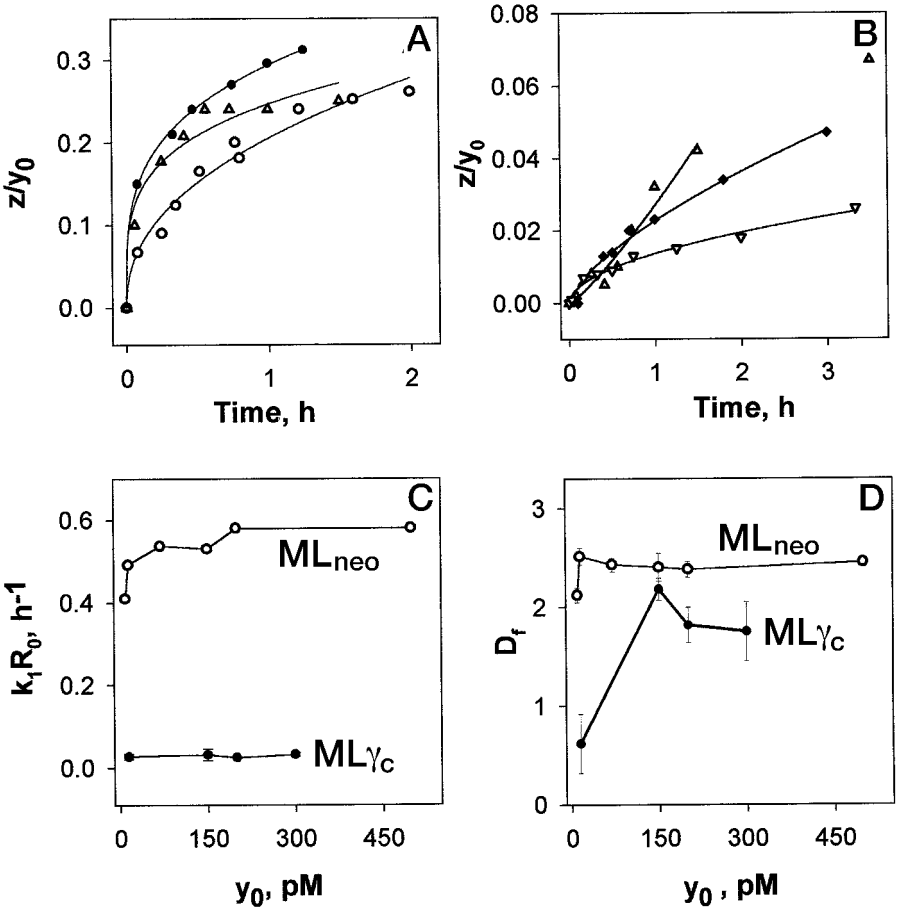

FIGURE 3 Dose-dependence of specific binding of ^{125}I-IL-13 (specific bound/total ^{125}I-IL-13, z/y_0) on ML_{neo} (*A*) and MLγ_c-transfected (*B*) RCC cells, integral rate binding (*C*) and fractal dimension parameter *(D)* at various ligand concentration. *(A)* 0.5×10^6 cells and 10 pM (—○—), 15 pM (—△—), and 500 pM (—●—) ^{125}I-IL-13; *(B)* 10^6 cells and 15 pM IL-13 (— —), 10^6 cells and 200 pM IL-13 (—◆—), and 0.5×10^6 (—▽—) 300 pM ^{125}I-IL-13. Kinetic binding studies were performed as described in Fig. 1. Bound ^{125}I-IL-13 was plotted as the ratio of specific bound ligand to the total radiolabeled ligand after subtraction of the nonspecifically bound fraction as described in Materials and Methods. Values represent the average of duplicate determinations: SEM values for each point are not shown to simplify presentation. The values of SD of the mean were not larger than 0.07. Experiments were repeated two times. The values of SD smaller than size of the points were not presented on the figures *C* and *D*.

number of binding sites on the cell surface or both. The kinetic fractal model described in Eq. 3 did not allow us to discriminate between these possibilities.

We used association and dissociation measurements at different initial concentrations of IL-13 to evaluate the association rate (k_1), dissociation rate (k_{-1}) and the number of binding sites per cell. We calculated these parameters using the simple one-receptor model (Eq. 2). Dissociation and binding kinetic experiments were performed using the same experimental protocol. This model fit our binding kinetics data in both control and γ_c-transfected ML-RCC cells at each initial concentration of ^{125}I-IL-13, taken separately to fit the mathematical model. Figure 4 shows the fit of this model at low (15 pM) IL-13 concentration. The analysis shows that, following γ_c transfection, the number of IL-13-specific binding sites on the cell surface was reduced and the affinity of this binding site decreased. These differences were defined at different initial concentrations of IL-13 and cells. However, we found that the estimated parameters, k_1 and R_0, changed monotonically with ligand concentration in both cell lines (Fig. 5 *A* and *B*). The rate of these changes differed in control and γ_c-transfected cells as a function of ligand concentration. At a low concentration of IL-13 (10–15 pM), a small number (330–440 sites per cell) of super-high affinity binding sites ($K_d = k_{-1}/k_1 \simeq 0.1$ pM) was estimated to exist on ML_{neo} cells, and a small number (170 sites per cell) of very high affinity binding sites ($K_d = 1.4 - 10$ pM) on $ML\gamma_c$ cells. At higher concentrations of IL-13, the number of binding sites increased for both RCC cell lines. These alterations of the number of binding sites and the association rate constant at various concentrations of ligand with an invariant rate of dissociation cannot be explained by a one-binding site ligand-receptor model.

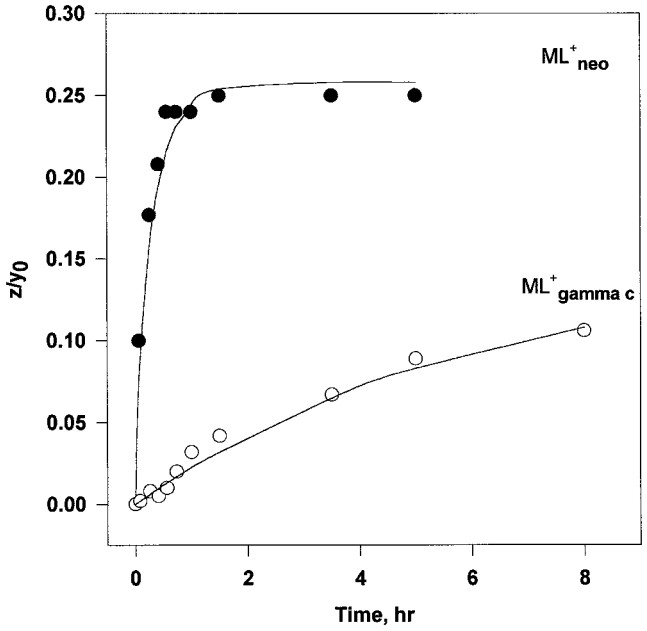

FIGURE 4 Association kinetic data and theoretical curves for ^{125}I-IL-13 binding. 15 pM ^{125}I-IL-13 was incubated with 0.5×10^6 ML_{neo} and 10^6 γ_c-transfected RCC cells at 4°C. Association kinetics was determined as described in Material and Methods. *Closed circles*, ML_{neo} RCC; *open circles,* $ML\gamma_c$-RCC. Symbols represent the mean values. Theoretical curves (*solid lines*) were generated by the model, Eq. 2, after fitting theoretical curves to experimental points. These curves were calculated at (1) $k_1 = 0.36$ (h pM)$^{-1}$, $k_{-1} = 0.023$ h^{-1}, $R_0 = 440$ sites per cell in the case of ML_{neo} RCC cells and (2) $k_1 = 0.0094$ (h pM)$^{-1}$, $k_{-1} = 0.014$ h^{-1}, $R_0 = 170$ sites per cell in the case of γ_c-transfected RCC cells. The amounts of dissociation rate constants, k_{-1}, were determined from analysis of dissociation assay (see Fig. 2).

Analysis of ligand concentration dependence of binding kinetics with Berg-Pursell model

The Berg-Pursell diffusion limit model (Berg and Pursell, 1977) was successfully used to explain the dependence of apparent association rate and apparent dissociation rate on the number of receptor molecules for some ligand-receptor systems (Erickson et al., 1987; Goldstein et al., 1989; Posner et al., 1992). According to the Berg-Pursell model, the ligand diffuses to a smooth spherical cell, closely approaches the cell surface, and forms a reversible complex with receptor sites. It was assumed that total concentrations of receptor and ligand does not change during the process. If the receptor has one binding site for ligand and the ligand-receptor complexes are in quasisteady state, then the apparent association rate coefficient and the apparent dissociation rate coefficient were modeled as

$$k_1 = k_{on}/(1 + Rk_{on}/k_+), \quad (8)$$

$$k_{-1} = k_{off}/(1 + Rk_{on}/k_+)), \quad (9)$$

$$R = x/N_c = R_0\varphi_{free} = (x_0/N_c)(1 - (1 - y/y_0)y_0/x_0), \quad (10)$$

where R is the average number of free binding sites on the cell surface; x, y are the concentrations of free ligand and free membrane receptor at steady state, respectively; x_0, y_0 are the initial concentrations of receptor and ligand, respectively; N_c is the number of cells per mL; R_0 is the average number of binding sites per cell; and φ_{free} is the fraction of free binding sites (i.e., $\varphi_{free} = x/x_0 = 1 - (y_0 - y)/x_0$); k_{on} and k_{off} are the fundamental rate constants of association and dissociation; k_+ is the diffusion limited forward rate constant, and $k_+ = 4\pi Da$, where a is the radius of a cell and D, is the diffusion coefficient of the ligand.

According to these equations, the effective rate of association must increase, when the initial concentration of ligand is increased. This is reasonable, because a higher concentration of ligand reduces the local concentration gradient (i.e., concentration change) of ligand near the cell surface and leads to the occupation of more receptor molecules. Furthermore, increasing the ligand concentration abolishes the diffusion limit. Therefore,

$$\lim_{y_0 \to \infty} k_1(y_0) = k_{on}.$$

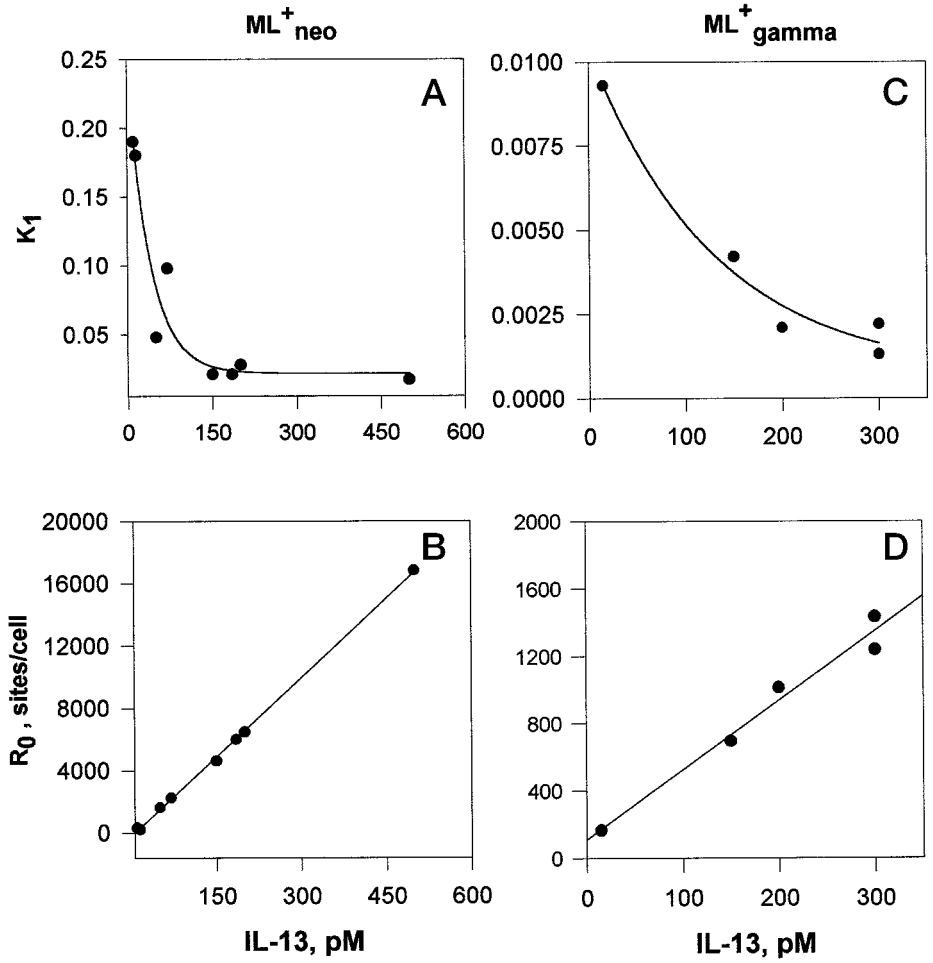

FIGURE 5 The ^{125}I-IL-13 concentration dependence of k_1, R_0 in the ML_{neo} *(A, B)* and $ML\gamma_c$ *(C, D)* RCC cells. The decrease of parameter k_1 was fitted to the exponential model; the increase in a number of available binding sites, R_0, at IL-13 concentration was fitted to a linear regression model.

The parameter, k_{-1}, follows the same type of dependence on y_0 as was shown for k_1: it must increase with increasing ligand concentration.

Our observations of dependence of the parameters k_1, k_{-1} on the initial ligand concentration disagreed with the predictions of dose-dependence for these parameters by the Berg-Pursell model. Figures 2 and 3 shows k_1 decreasing and k_{-1} independent of the initial concentration of IL-13. This behavior was found for both ML_{neo} and $ML\gamma_c$ cells. We also observed the same behavior at much higher concentrations of ligand (50–200 pM ^{125}I-IL-13 and 50–100 nM unlabeled IL-13).

Numerical analysis of Eqs. 8–10 shows that the kinetic parameters k_{on} and k_1 are very similar for concentrations of IL-13 from 10 to 500 pM. For example, for ML_{neo} cells, when $y_0 = 10$ pM, $D = 10^{-6}$ (cm^2/s), $a \simeq 4$ μm; then $k_+ = 1.09 \times 10^4$ (pM h)$^{-1}$ $= 5.02 \times 10^{-9}$ (cm^3/s) $= 3 \times 10^{12}$ (s M)$^{-1}$; $k_1 = 5.3 \times 10^7$ (s M)$^{-1}$; $\varphi_{free} = [1 - (0.25 \times 10)/2.75] = 0.089$; $R = 330 \times \varphi_{free} = 0.089 \times 330 = 29$ copies/cell; $k_f \times R = (5 \times 10^7)29 = 1.5 \times 10^9$. Thus, $k_{on} \simeq 5.5 \times 10^7$ (s M)$^{-1}$ $= k_1$.

Similar results were obtained for other initial concentrations of IL-13. These results suggest that ligand diffusion did not limit the binding step of the reaction. Thus, the diffusion step in two-step binding kinetics (diffusion + binding of ligand) is negligible for IL-13 binding.

A two-independent receptor model in γ_c-transfected ML-RCC cells

Because γ_c-transfection abolishes the dependence of IL-13R binding rate on the concentration of IL-13, and the dissociation curves demonstrate a very fast and a very slow phase, it was reasonable to assume that binding, dissociation, and displacement curves could be described by a two-independent binding site model (Eq. 4, Tables 1 and 2).

Figure 6 shows that the model by Eq. 4 can fit the binding and dissociation kinetic curves at different concentrations of ligand. These results indicate that ML_{γ_c} cells express intermediate-affinity (R_{10}) and high-affinity (R_{20}) binding sites. $R_{10} = 3030 \pm 2300$ copies/cell and $R_{20} = 560 \pm 60$ copies/cell. The association rate and dissociation rate constants for the first type of receptor were $k_1 = 1.5 \times 10^{-3}$ (h pM)$^{-1}$ and $k_{-1} = 5.0 \pm 4.0$ h^{-1}. The kinetic constants for the second type of receptor were $k_2 = 1.9 \times 10^{-3} \pm 0.2 \times 10^{-3}$ $(h\,pM)^{-1}$, and $k_{-2} = 0.015 \pm 0.004$ h^{-1}. The parameters were evaluated with the fitting procedure as

TABLE 1 Equations for mathematical models of IL-13 and IL-13 receptor interactions for ML-RCC cells without and with γ_c-chain expression

Control Cells	γ_c-Expressed Cells
Binding Assay	
$dz(t)/dt = (n_1 y^b)yx - n_{-1}z - dz_c(t)/dt$	$dz_1(t)/dt = k_1 x_1 y - k_{-1} z_1$
$dz_c(t)/dt = n_2 zc - n_{-2} z_c$	$dz_2(t)/dt = k_2 x_2 y - k_{-2} z_2$
$di(t)/dt = n_4 z_c - dy_i(t)/dt$	
$dy_i(t)/dt = n_3 iy - n_{-3} y_i$	
$x(t) = x_0 - z(t) - z_c(t)$	$x_1(t) = x_{10} - z_1(t)$
$c(t) = c_0 - z_c(t)$	$x_2(t) = x_{20} - z_2(t)$
$y(t) = y_0 - z(t) - z_c(t) - y_i(t)$	$y(t) = y_0 - z_1(t) - z_2(t)$
$A_c(t) = [z(t) + z_c(t)]/y_0$	$A(t) = [z_1(t) + z_2(t)]/y_0$
Dissociation Assay	
$dz(t)/dt = -n_{-1}z - dz_c(t)/dt$	$dz_1(t)/dt = -k_{-1} z_1$
$dz_c(t)/dt = n_2 zc - n_{-2} z_c$	$dz_2(t)/dt = -k_{-2} z_2$
$c(t) = c_0 - z_c(t)$	
$B_c(t) = [z(t) + z_c(t)]/[z(\tau) + z_c(\tau)]$	$B(t) = [z_1(t) + z_2(t)]/[z_1(\tau) + z_2(\tau)]$
Displacement Assay	
$dz(t)/dt = (n_1 y^b)yx - n_{-1}z - dz_c(t)/dt$	$dz_1(t)/dt = k_1 x_1 y - k_{-1} z_1$
$dq(t)/dt = (n_1 y_1^b) y_1 x - n_{-1} q - dq_c(t)/dt$	$dq_1(t)/dt = k_1 x_1 y_1 - k_{-1} z q_1$
$dz_c(t)/dt = n_2 zc - n_{-2} z_c$	$dz_2(t)/dt = k_2 x_2 y - k_{-2} z_2$
$dq_c(t)/dt = n_2 qc - n_{-2} q_c$	$dq_2(t)/dt = k_2 x_2 y_1 - k_{-2} q_2$
$di(t)/dt = n_4(z_c + q_c) - dy_i(t)/dt - dy_{1i}/dt$	
$dy_i(t)/dt = n_3 iy - n_{-3} y_i$	
$dy_{1i}(t)/dt = n_3 iy_1 - n_{-3} y_{1i}$	
$x(t) = x_0 - z(t) - z_c(t) - q(t) - q_c(t)$	$x_1(t) = x_{10} - z_1(t) - q_1(t)$
$c(t) = c_0 - z_c(t) - q_c(t)$	$x_2(t) = x_{20} - z_2(t) - q_2(t)$
$y(t) = y_0 - z(t) - z_c(t) - y_i(t)$	$y(t) = y_0 - z_1(t) - z_2(t)$
$y_1(t) = y_{10} - q(t) - q_c(t) - y_{1i}(t)$	$y_1(t) = y_{10} - q_1(t) - q_2(t)$
$C_c(t) = [z(t) + z_c(t)]/[\bar{z}(t) + \bar{z}_c(t)]$	$C(t) = [z_1(t) + z_2(t)]/[\bar{z}_1(t) + \bar{z}_2(t)]$
Internalization Assay	
$dz_f(t)/dt = -\kappa_1 z_f - \kappa_{in} z_f$	
$dz_s(t)/dt = -\kappa_2 z_s$	
$dz_{out}(t)/dt = \kappa_1 z_f + \kappa_2 z_s$	
$dz_{in}(t)/dt = \kappa_{in} z_f$	
$C_s(t) = [z_f(t) + z_s(t)]/[z_f(\tau) + z_s(\tau)]$;	
$C_{in}(t) = z_{in}(t)/[z_f(\tau) + z_s(\tau)]$; $C_{out}(t) = z_{out}(t)/[z_f(\tau) + z_s(\tau)]$	

(See definitions in Table 2).

described in Material and Methods. The dissociation constants for intermediate-affinity and high-affinity receptors were estimated as $K_1 = k_{-1}/k_1 = 3.3$ nM and $K_2 = k_{-2}/k_2 = 8$ pM. We also investigated the accuracy of the estimated parameters by fitting the model with displacement assay data. Figure 6 *D* shows that our model agrees with the displacement assay protocol. The numerical values of the parameters of the model were the same, which was found by fitting the binding/dissociation kinetic data.

Analysis of potential models of IL-13 binding in ML_{neo} γ_c-negative cells

We also applied a two-binding site model to simultaneously fit binding and dissociation kinetic curves on ML_{neo} RCC cells at different concentrations of radiolabeled ligand. However, this model did not accurately describe the kinetic binding experiments at different concentrations of ligand (data not shown). We also tried to improve fitting by using an advanced nonsteady-state diffusion-reaction model (Goldstein and Dembo, 1995). This model took into account diffusion-controlled binding of ligand to two receptor populations and included the possibility of rebinding of ligand after dissociation from each type of receptor. However, this model was also rejected by goodness-of-fit statistical analysis.

Neither a three-independent receptor binding site model nor a model of homodimerization of IL-13R induced by ligand binding fit our set of experimental data. We also modified a two-binding site model so that a fraction of a receptor could bind to more than one IL-13 molecule. However, the goodness of fit analysis revealed a poor fit of this model (data not shown).

A model of ligand-induced coreceptor mediated binding in ML_{neo} RCC cells

Because neither simple one-site model or other conventional models adequately fit the set of binding and dissociation data, a cooperative binding model was tried. We postulated that the association rate is a nonlinear function of free ligand concentration, so that the binding rate is increased (or decreased) over time while binding occurs. We also proposed that a third molecule, dubbed the coreceptor

TABLE 2 Definitions and typical units of all variables and parameters of this work

Symbol	Definition	Units
x	Unbound cell surface receptor molecules concentration	nM
y	Free ligand molecules concentration	nM
z	Cell surface ligand–receptor complexes concentration	nM
c	Unbound cell surface coreceptor molecules concentration	nM
z_c	Cell surface ligand–receptor–coreceptor complexes concentration	nM
y_1	Free (unlabeled) ligand-competitor complexes concentration	nM
i	Free inhibitor molecules concentration	nM
y_i	Ligand–inhibitor complexes concentration	nM
y_{1i}	Ligand-competitor–inhibitor complexes concentration	nM
q	Cell surface ligand-competitor–receptor complexes concentration	nM
q_c	Cell surface ligand-competitor–receptor–co-receptor complexes concentration	nM
y_0	Initial ligand molecules concentration	nM
x_0	Initial cell surface receptor molecules concentration	nM
z_0	Initial cell surface ligand–receptor complexes concentration	nM
c_0	Initial cell surface coreceptor molecules concentration	nM
z_{c0}	Initial cell surface ligand–receptor–coreceptor complexes concentration	nM
y_{10}	Initial (unlabeled) ligand-competitor concentration	nM
i_0	Initial free inhibitor molecules concentration	nM
y_{i0}	Initial ligand–inhibitor complexes concentration	nM
y_{1i0}	Initial ligand-competitor–inhibitor complexes concentration	nM
q_0	Initial cell surface ligand-competitor–receptor complexes concentration	nM
q_{c0}	Initial cell surface ligand-competitor–receptor–coreceptor complexes concentration	nM
y_{10}	Initial ligand-competitor complexes concentration	nM
A_c	A fraction of bound ligand (observed variable) in binding assay	none
B_c	A fraction of bound ligand (observed variable) in dissociation assay	none
C_c	A fraction of bound ligand (observed variable) in displacement assays	none
$\bar{z} + \bar{z}_c$, $\bar{z}_1 + \bar{z}_2$	Bound ligand concentration at the absence of ligand-competitor (i.e., at $y_{10} = 0$)	nM
x_1	Concentration of the unbound cell surface copies of the type 1 receptor	nM
x_2	Concentration of the unbound cell surface copies of the type 2 receptor	nM
z_1	Cell surface ligand–receptor type 1 complex concentration	nM
z_2	Cell surface ligand–receptor type 2 complex concentration	nM
q_1	Cell surface ligand-competitor–receptor type 1 complex concentration	nM
q_2	Cell surface ligand-competitor–receptor type 2 complex concentration	nM
x_{10}	Initial concentration of the cell surface type 1 receptor molecules	nM
x_{20}	Initial concentration of the cell surface type 2 receptor molecules	nM
z_{10}	Initial cell surface ligand–receptor type 1 complex concentration	nM
z_{20}	Initial cell surface ligand–receptor type 2 complex concentration	nM
q_{10}	Initial cell surface ligand-competitor–receptor type 1 complex concentration	nM
q_{20}	Initial cell surface ligand-competitor–receptor type 2 complex concentration	nM
z_f	Unbound cell surface fast receptor molecules concentration	nM
z_s	Unbound cell surface slow receptor molecules concentration	nM
z_{in}	Internalized ligand–receptor complex molecules concentration	nM
z_{out}	Shed/dissociated ligand molecules concentration	nM
τ	Initial time point of dissociation assay or internalization assay	min
A	Fraction of bound ligand (the observed variables) in binding assay	none
B	Fraction of bound ligand (the observed variables) in dissociation assay	none
C	Fraction of bound ligand (the observed variables) in displacement assays	none
C_s	Fraction of cell surface bound ligand in internalization assay	none
C_{in}	Fraction of internalized ligand	none
C_s	Fraction of shed/dissociated ligand in internalization assay	none
t	Time	h
N_c	Concentration of cells	M^{-1}
R_0	Total number of binding sites per cell	#/cell
R	Total number of free binding sites per cell	#/cell
N_R	Number of receptor molecules per cell	#/cell
N_{C_0}	Number of coreceptors molecules per cell	#/cell
R_1	Number of type 1 receptor molecules per cell	#/cell
R_2	Number of type 2 receptor molecules per cell	#/cell
D	Diffusion coefficient	cm^2/s
D_f	Fractal dimension constant of cell surface	none
κ_f	Effective binding rate	h^{-1}
k_1	Rate constant for association of ligand–receptor complexes	$[h\ pM]^{-1}$
k_{-1}	Rate constant for dissociation of ligand–receptor complexes	h^{-1}
k_2	Rate constant for association of ligand–receptor complexes	$[h\ pM]^{-1}$
k_{-2}	Rate constant for dissociation of ligand–receptor complexes	h^{-1}

TABLE 2 Continued

Symbol	Definition	Units
n_1	Rate constant for association of ligand–receptor complexes	$[\text{h pM}]^{-1}$
n_{-1}	Rate constant for dissociation of ligand–receptor complexes	h^{-1}
n_2	Rate constant for association of ligand–receptor complex with coreceptor	$[\text{h pM}]^{-1}$
n_{-2}	Rate constant for dissociation of ligand–receptor complexes and coreceptor	h^{-1}
n_3	Rate constant for association of ligand–inhibitor complexes	$[\text{h pM}]^{-1}$
n_{-3}	Rate constant for dissociation of ligand–inhibitor complexes	h^{-1}
n_4	Rate constant for release of inhibitor molecules by cells	$[\text{h pM}]^{-1}$
k_{on}	Fundamental rate constant for binding	$[\text{h pM}]^{-1}$
k_{off}	Fundamental rate constant for dissociation	h^{-1}
k_+	Diffusion limited forward rate constant	$[\text{h pM}]^{-1}$
κ_1	Constant rate for shedding/dissociation of ligand–receptor type 1 complexes	h^{-1}
κ_2	Constant rate for shedding/dissociation of ligand–receptor type 2 complexes	h^{-1}
κ_{in}	Constant rate for internalization of ligand–receptor type 1 complexes	h^{-1}
κ'_{in}	Constant rate for internalization of ligand–receptor type 2 complexes	h^{-1}
a	Radius of a cell	μm
b	Cooperative binding parameter	none
K_{d}	Equilibrium dissociation constant	nM
N_{A}	The Avogadro number ($= 6.02 \times 10^{23}$)	#/mole
$t_{1/2}$	Half-time	h
ϕ_{free}	Fraction of free binding sites	none

subunit, exists and helps keep the ligand on the cell surface for a long period of time and causes the release of the inhibitor molecule(s). This inhibitor molecule drifts away from the cell membrane and binds to free IL-13 molecules in the medium, which are then captured so they cannot bind to receptors on the cell membrane. This last assumption is consistent with the fact that both small and large concentrations of IL-13 appear to have almost the same binding effect at the steady-state phase of reaction (Fig. 7 *A* and *B*). Based on these assumptions, we established the following model for IL-13 binding on the cell surface.

$$x + y \underset{n_{-1}}{\overset{n_1 y^b}{\rightleftharpoons}} z, \tag{11}$$

$$z + c \underset{n_{-2}}{\overset{n_2}{\rightleftharpoons}} z_c \xrightarrow{n_4} z_c + i, \tag{12}$$

$$y + i \underset{n_{-3}}{\overset{n_3}{\rightleftharpoons}} y_i, \tag{13}$$

where y, x, and c are the free (unbound) ligand (IL-13), free primary binding subunit, and free coreceptor, respectively; i is the inhibitor (released or shed from cell surface molecules); z and z_c are the complex $(x + y)$ and three-molecular complex $(c + x + y)$; y_i is the inactivated ligand, i.e., the $(y + i)$ complex. n_1 and n_{-1} are the association and dissociation constant rates of IL-13 to the primary binding subunit; n_2 and n_{-2} are the association and dissociation rate constants of the IL-13 bound primary receptor to the free coreceptor, respectively; n_3 and n_{-3} are the association and dissociation rates of the inhibitor to IL-13; and n_4 is the rate of release/shedding of the inhibitor from cells to medium.

A small but significant amount of cooperativity is present in reaction 11 (see also Fig. 3). This is modeled by assuming that the association constant for this reaction is of the form $n_1 y^b$ with $0 \le b < 1$, where b is the cooperative binding parameter of IL-13R expressed on the cell membrane. This parameter indicates the level of heterogeneity of binding capacity of binding sites on cell surfaces that can be correlated to the complexity (fractal dimension) of the cell surface. The complex shape of a cell membrane can impose a restraint on the binding of ligand to receptor molecules localized in inaccessible regions. The parameter b could also indicate the fraction of binding sites that pre-exist on the cell membrane in a homodimer and/or heterodimer form in the absence of external ligand. If $b = 0$, then the binding kinetics follows the classical mass laws kinetic reactions, if $b > 0$, then positive cooperativity in binding is expressed.

Table 1 contains a mathematical model of binding assays for IL-13–IL-13R interaction in control RCC cells. Note that, for the binding kinetic model, the constant y_0 is the initial concentration of ligand (pM), and x_0 (pM), and c_0 (pM) are the concentrations of primary binding sites and coreceptor copies, respectively, $z(0) = z_c(0) = y_i(0) = i(0) = 0$.

By fitting differential equations for reactions 11–13 to our set of binding and dissociation data (Fig. 7) at different initial concentrations of IL-13, we estimated the set of constants x_0, c_0, n_1, n_{-1}, n_2, n_{-2}, n_3, n_{-3}, n_4, and b. The average number of binding sites and average number of coreceptor copies per cell was evaluated by Eqs. $N_R = x_0/N_c$ and $N_{C_0} = c_0/N_c$, where N_c is the concentration of target cells. When we applied the fitting procedure, we found high correlations between estimated values x_0, and c_0, as well as between a few other estimated parameters. In other words, the available experimental data allowed estimation of the

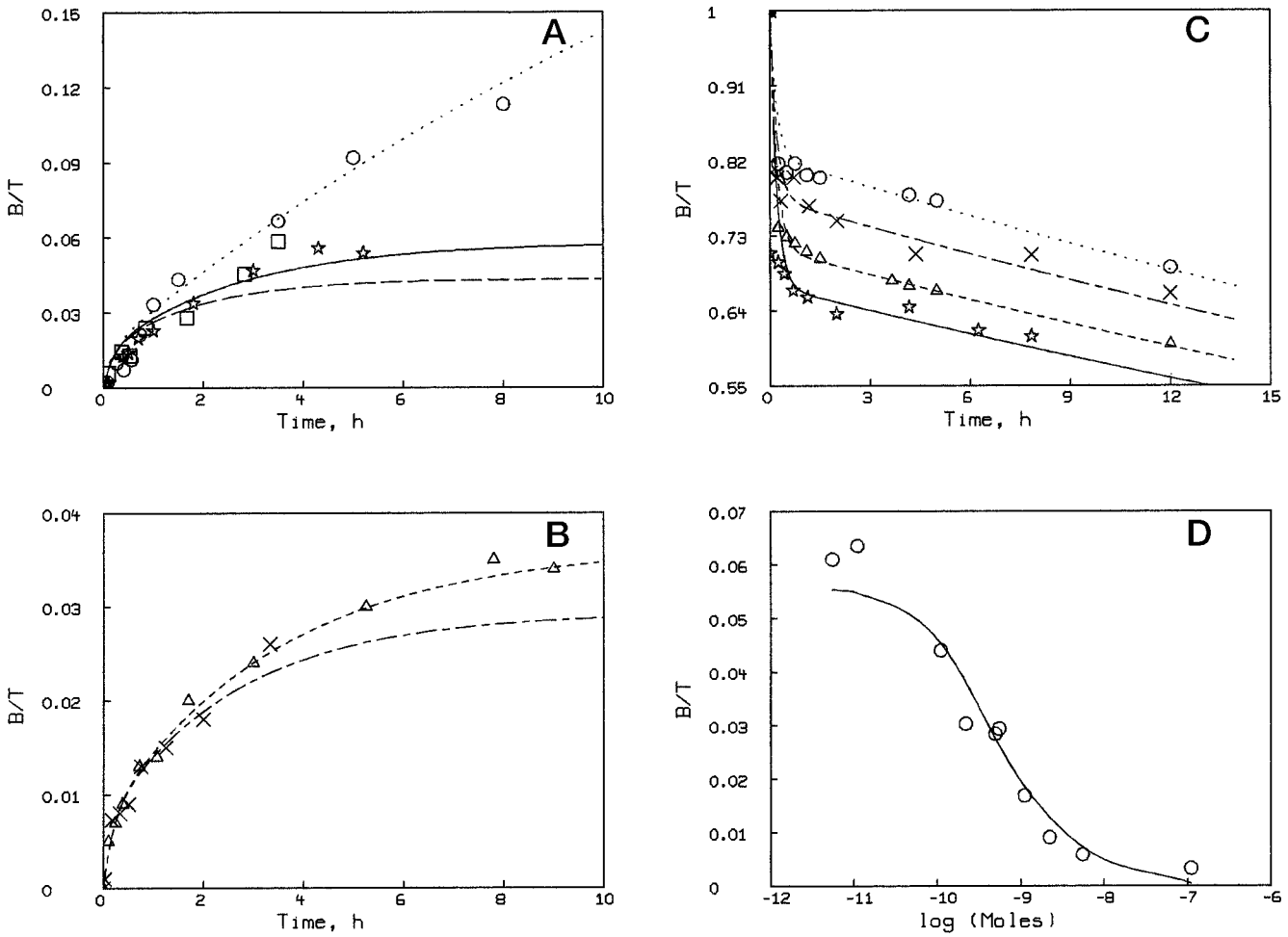

FIGURE 6 Fitting of two-independent receptor model. Association of IL-13 to the surface receptors (*A*, *B*), dissociation of IL-13 (*C*) from the cell membrane, and a numerical prediction of displacement curve (*D*) in the MLγ_c RCC is shown. The initial conditions were: (*A*) $y_0 = 15$ pM, $N_c = 10^6$ cell/mL (-○-); $y_0 = 200$ pM, $N_c = 1.0 \times 10^6$ cell/mL (–☆–), $y_0 = 300$ pM, $N_c = 1 \times 10^6$ cell/mL (--□--); (*B*) $y_0 = 150$ pM, $N_c = 0.5 \times 10^6$ cells/mL (--△--), $y_0 = 200$ pM, $N_c = 0.5 \times 10^6$ cells/mL (--×--), (*C*) $y_0 = 15$ pM, $N_c = 10^6$ cell/mL (--○--); $y_0 = 150$ pM, $N_c = 0.5 \times 10^6$ cell/mL (--△--); $y_0 = 200$ pM, $N_c = 0.5 \times 10^6$ cell/mL (--×--); $y_0 = 200$ pM, $N_c = 10^6$ cell/mL (–☆–); $\tau = 4$ *h* (*D*) Displacement assays were performed in separate experiments, 10^6 cell ML_{neo} cells were incubated with 100 pM ^{125}I-IL-13 in the absence or presence of different concentrations of unlabeled IL-13 (from 5 pM to 110 nM) at 3.5 h. The lines show theoretical curves.

ratio of these parameters but not their values individually. This parametrization property often limits the predictive power of kinetic models. Therefore, to reduce the number of calculated parameters and their correlations, we fixed a mean of parameters x_0, n_{-1}, n_2, and n_3. The number of binding sites per cell, R_0 ($R_0 = x_0/N_c$ or concentration of IL-13 receptor (x_0)), on the control ML_{neo} cells have been previously evaluated using a one-receptor model (Obiri et al., 1996b). This number varied from 360×10^3 to 620×10^3 molecules/cell. We assumed that $N_R = 360 \times 10^3$ molecules/cell. The constant, n_{-1}, was estimated by fitting the two-binding site model (see Eq. 6) to the set of dissociation curves. The amount of rate constants n_3 ($n_3 = 4$ (h pM)$^{-1}$) and n_2($n_2 = 1.22 \times 10^{-4}$ (h pM)$^{-1}$) were taken from the best set of constants when we applied the fitting procedure for evaluation of complete set of constants, i.e., x_0, c_0, n_1, n_{-1}, n_2, n_{-2}, n_3, n_{-3}, n_4, and b. Finally, we simultaneously estimated 6 constants: c_0, n_1, n_{-2}, n_{-3}, n_4, and b, using about 60 duplicate experimental points of 7 kinetic curves.

Figure 7 shows the result of fitting of the mathematical model for reactions 11–13 using the best set of parameters: $c_0 = 5587 \pm 222$ pM (or $N_{C_0} = 336 \times 10^3 \pm 14 \times 10^3$ molecules/cell); $n_1 = 3.36 \pm 0.25 \times 10^{-4}$ (h pM)$^{-1}$; $n_{-1} = 4.8$ h^{-1}; $n_2 = 1.22 \times 10^{-4}$ (h pM)$^{-1}$; $n_{-2} = 0.023 \pm 0.001$ h^{-1}; $n_{-3} = 0.23 \pm 1.55$ h^{-1}; $n_3 = 4 \pm 8$ (h pM)$^{-1}$; $n_4 = 0.83 \pm 0.05$ h^{-1}; $b = 0.09 \pm 0.015$.

These results show that a large number of coreceptor molecules are expressed on the cell surface of control ML_{neo} cells. The effective rate of ligand association to primary receptor ($n_1 x_0 = 2.0$ h^{-1}) is 3 times higher than the effective rate of capture of ligand-receptor complexes by coreceptor ($n_2 c_0 = 0.68$ h^{-1}). The dissociation constant of the primary receptor, coreceptor, and inhibitor complexes differed dra-

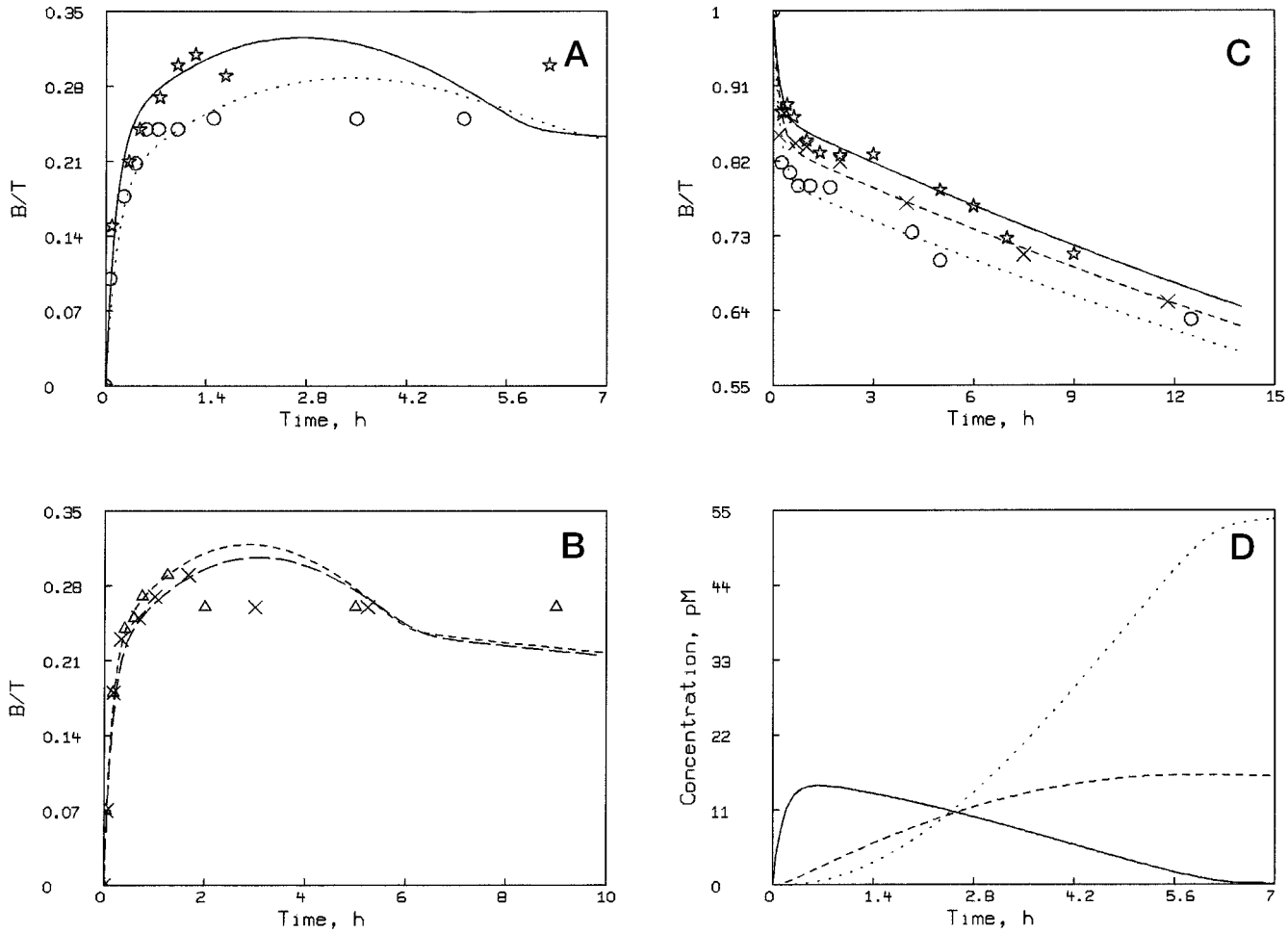

FIGURE 7 (*A*, *B*) ^{125}I-IL-13 binding kinetics, (*C*) dissociation kinetics, and (*D*) simulation of time course of separate variables of mathematical model. Kinetics of binding experimenters were performed at various initial concentrations of radiolabeled IL-13 such as (*A*) y_{01} = 15 pM (○), y_{02} = 500 pM (☆). (*B*) y_{03} = 70 pM (△), y_{04} = 200 pM (×). (*C*) Dissociation experiments were performed at y_{05} = 15 pM, (○), y_{06} = 200 pM (×), y_{07} = 500 pM (☆) τ = 5 h. The values of SD and mean were not larger than 0.07. Kinetic binding and dissociation studies were performed as described in Figs. 1 and 2. The lines are the theoretical kinetic curves. Kinetics of the ligand receptor complex ($z = [x + y]$) (*solid line*), three-molecular complex ($z_c = [y + x + c_0]$) (*dash line*) and inhibitor (*i*) (*dot line*) are shown at the initial conditions: (*D*) y_0 = 15 pM; x_0 = 5980 pM, c_0 = 5587 pM; $z = z_c = y_i = i = 0$.

matically: $K_{dR} = n_{-1}/n_1 = 14.3$ nM, $K_{dC_0} = n_{-2}/n_2 = 188$ pM, $K_{di} = n_{-3}/n_3 = 0.06$ pM, respectively.

IL-13 displacement analysis in ML_{neo} cells

Because our model suggested a new control mechanism mediated by the postulated coreceptor component, it was important to determine if our model was accurate, and if the parameter estimations were stable over a broad range of IL-13 concentrations. We designed binding and displacement assays simultaneously in the same experimental protocol (Fig. 8). We used 50 pM ^{125}I-IL-13, and the concentration of unlabeled IL-13 was varied from 5 pM to 200 nM. The model for the displacement assay was constructed from Eqs. 11–13 for radiolabeled ligand binding and by the schema

$$x + y_1 \underset{n_{-1}}{\overset{n_1 y_1^b}{\rightleftharpoons}} q, \tag{14}$$

$$z + c \underset{n_{-2}}{\overset{n_2}{\rightleftharpoons}} q_c \overset{n_4}{\longrightarrow} q_c + i, \tag{15}$$

$$y_1 + i \underset{n_{-3}}{\overset{n_3}{\rightleftharpoons}} y_{1i}, \tag{16}$$

for unlabeled IL-13 binding. Where y_1 is free (unbound) unlabeled IL-13; q and q_c are the complex ($x + y_1$) and three-molecular complex ($c + x + y_1$); i is the inhibitor produced after binding of the coreceptor with ligand-receptor complex q; y_{1i} denotes inactivated unlabeled ligand. Corresponding mathematical model is presented in Table 1.

The five relatively sensitive parameters n_1, n_2, n_3, n_4, and b were estimated along with fixed parameters (n_{-1} = 4.8 h^{-1}, n_{-2} = 0.023 h^{-1}, n_{-3} = 0.23 h^{-1}, x_0 = 5980 pM, c_0 = 5587 pM) by fitting the binding and displacement assays. The result of simultaneously fitting the model for the binding/dissociation reactions described in Eqs. 11–13 (Fig. 8 *A*)

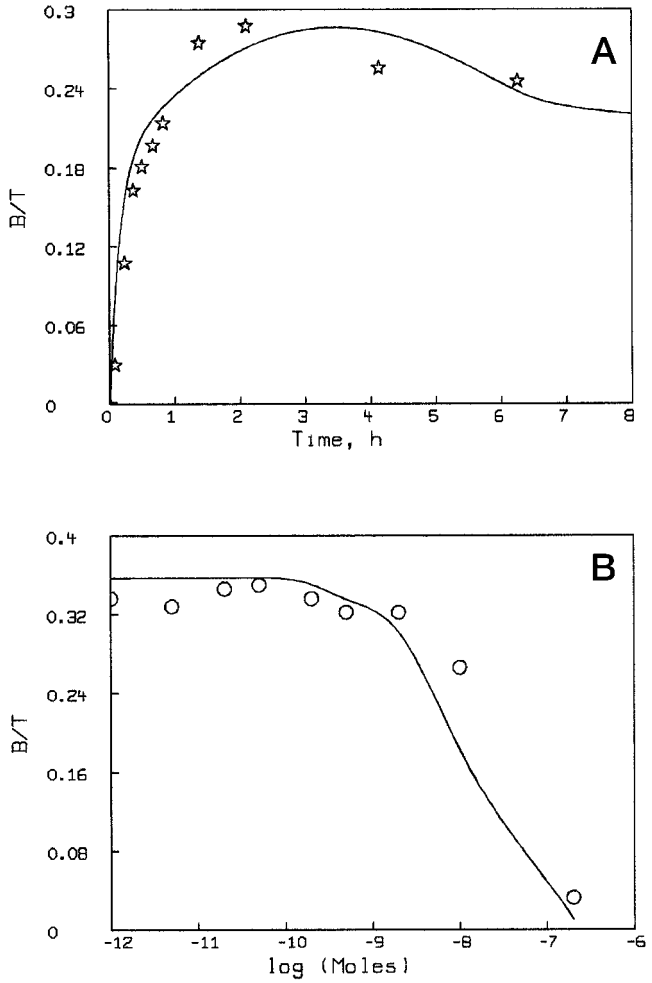

FIGURE 8 ^{125}I-IL-13 association and displacement assays. The association kinetic experiments were performed using 50 pM ^{125}I-IL-13 and 0.5×10^6 ML_{neo} cells. (*A*) Displacement assays were performed using 85 pM ^{125}I-IL-13, 1×10^6 ML_{neo} cells and various concentrations of unlabeled IL-13 (from 5 pM to 200 nM) for 2.7 h incubation at 4°C. (*B*) The numerical solutions were derived from the model, Eqs. 11–13, (*A*), 14–16 and are shown by solid lines. The values of SD of the mean were not larger than 0.07.

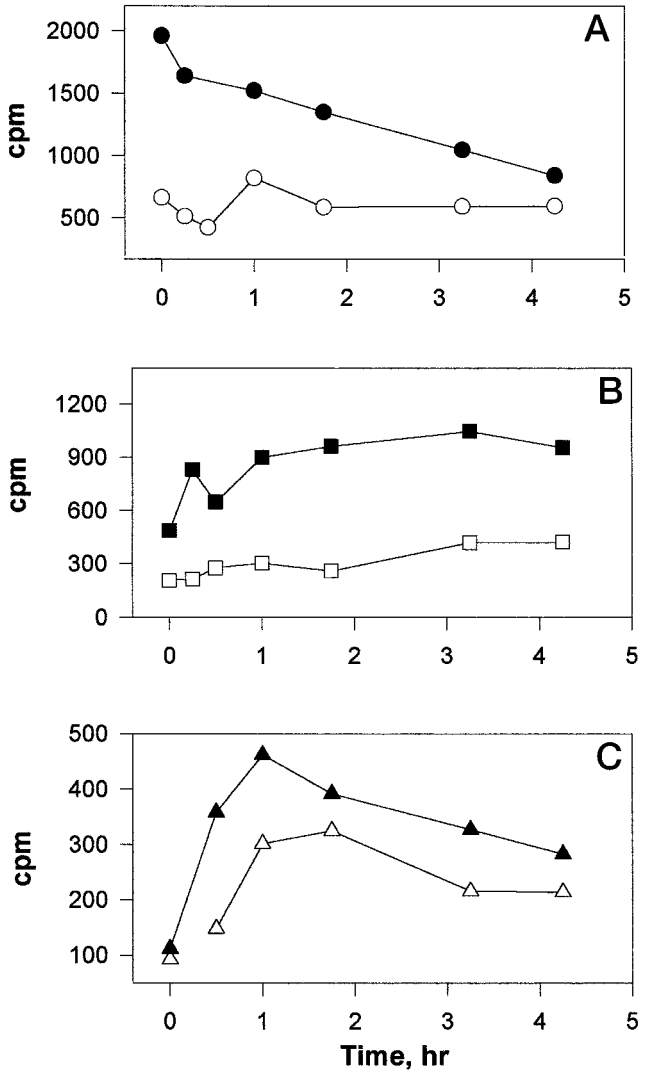

FIGURE 9 IL-13R-mediated dissociation/shedding and internalization of ^{125}I-IL-13. Control (*filled symbols*) and γ_c transfected (*open symbols*) ML-RCC cells (2.4×10^6) were preincubated for 5 min in binding buffer containing 0.2 nM chloroquine at 37°C and then incubated in the same volume with 300 pM ^{125}I-IL-13 for 3.5 hr at 4°C. Cells were washed two times and the temperature was then raised to 37°C. At various time intervals, two duplicate sets of 50 μL aliquots were taken. One set was incubated with glycine buffer (final pH = 2.0) for 10 min. The suspension was then centrifuged through a mixture of phthalate oils and the radioactivity in the supernatant (*A*, surface bound + dissociated) and in the cell pellet (*C*, acid resistant or internalized) was determined with a gamma counter. The other set of 50 μL aliquots (*B*) was directly centrifuged through phthalate oils and the radioactivity observed in the supernatant was used for dissociated ^{125}I-IL-13 values.

and the model for the displacement reactions Eqs. 11–16 (Fig. 8 *B*) demonstrates that our model agrees with these sets of observations. A mathematical model for Eqs. 11–13, and 14–16 fits data using parameters that are very similar to parameters described in Fig. 7.

Thus, we can conclude that our stoichiometric model, 11–13, can describe IL-13–IL-13R binding on cells that do not express γ_c, at least for concentrations of IL-13 from 10 pM to 200 nM.

Internalization of ^{125}I-IL-13

As shown in Fig. 9, the rate of internalization and dissociation/shedding of IL-13 at 37°C was higher for control cells. However, the relative distribution of ^{125}I-IL-13 on the cell surface, within cells, and in the medium were similar. Similar internalization and dissociation/shedding was observed for another RCC cell line (HL-RCC). Figure 10 shows the kinetics of ^{125}I-IL-13 binding on the cell surface, fraction remaining inside the cell, and unbound radiolabeled IL-13 in the cell culture medium for HL, ML_{neo}, and $ML\gamma_c$-transfected RCC cell lines. Kinetic data are shown after normalization. IL-13 internalization kinetics in all types of cell lines was similar. The solid lines show the numerical solutions according to the two-state receptor model

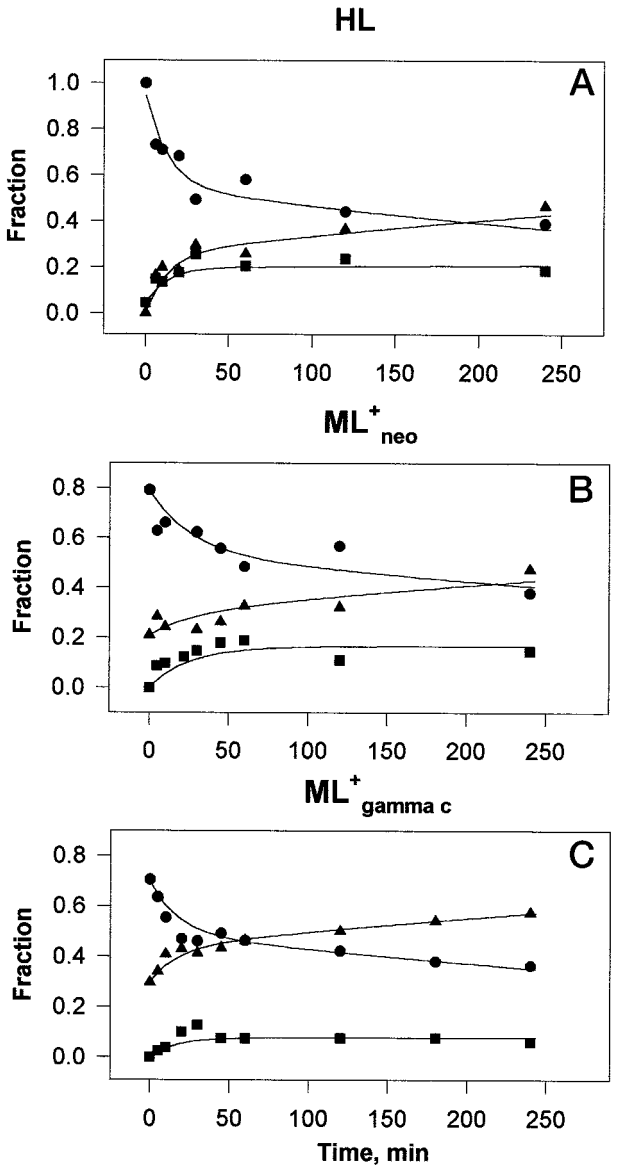

FIGURE 10 Endocytosis and dissociation/shedding of surface bound ^{125}I-IL-13 by RCC cells. (*A*) HL, (*B*) ML_{neo}, and (*C*) $ML\gamma_c$ cells (1.8×10^6) were processed and incubated as described in Fig. 9. Fractions of specific surface-bound (–●–), internalized (–■–) and shed/dissociated ligand (–▲–) were calculated by the formula presented in Materials and Methods. Kinetic parameter values are listed in the Table 3. The results were reproduced in two separate experiments.

(Kuznetsov, 1990; Kuznetsov and Borisova, 1995b). Only 15–25% and 12–17% of total bound radiolabeled ligand is internalized by control and γ_c-transfected RCC cells, respectively. The same fractions were dissociated or shed from cell surfaces. Internalization in these cell lines was ceased after 20–45 min. After this period, a fraction of internalized ligand stayed at the steady-state level within the cell for at least 4.5 hours. These results indicate that two types of IL-13R or conformation states of single IL-13R might exist on the surface of HL, ML_{neo}, and γ_c-transfected RCC cells, which differ in their rate of internalization and dissociation/shedding. The two-state receptor model, Eq. 4 [but not the one-state receptor model (data not shown)], provided the best fit for all experimental data (Fig. 10). The estimations of the kinetic parameter values κ_1, κ_2, κ_{in}, κ_{out}, and the ratio between fast and slow forms of IL-13R at quasisteady state of binding, $z_{f_0}/(z_{f_0} + z_{s_0})$, are listed in Table 3. These data indicate that γ_c does not affect IL-13 internalization, but that it accelerates the shedding/dissociation of the fast form of IL-13R in RCC cells compared to γ_c-negative control RCC cells. In addition, the ratio between fast and slow forms of IL-13R at quasisteady state of binding is unchanged by γ_c-transfection.

Table 1 summarizes the models for IL-13–IL-13R interaction in cells without and with γ_c-expression. In the table, we included the functions $A(t)$, $A_c(t)$, $B(t)$, $B_c(t)$, $C(t)$, $C_c(t)$, $C_s(t)$, $C_{in}(t)$, C_{out}, which were used for fitting of the models to experimental data. Table 2 contains the definitions and dimension of the variables and parameters of our models.

Effect of γ_c expression on growth kinetics of RCC cells

To assess the physiological significance of expression of γ_c, we compared the growth of control and $ML\gamma_c$-transfected cells. Figure 11 shows that growth rate of $ML\gamma_c$-transfected cells is about two times higher than the growth rate of negative control ML_{neo} cells. Thus, reducing IL-13R expression on transfected cells correlates with enhancement of RCC growth.

DISCUSSION

This is the first report describing the kinetics of binding, dissociation, and internalization of IL-13 after binding to its receptors. We describe a new phenomenon associated with the IL-13 receptor where the apparent rate of association, but not dissociation, is strongly related to IL-13 concentration. The dissociation curves show both a fast and a very slow decay phase. Binding and dissociation assays indicate that IL-13R exists in both high-affinity (K_d = 188 pM) and intermediate-affinity (K_d = 14 nM) forms on ML_{neo} RCC cells and in very high affinity (K_d = 8 pM) and intermediate affinity (K_d = 3.3 nM) forms on γ_c-transfected cells. These data agree with displacement assays using unlabeled ligand as a competitor. Our results lead to the assumption that the dominant kinetic mechanism for IL-13R may depend on the initial concentration of ligand, and on topological and physical properties of the cell membrane.

TABLE 3 Parameters and estimates for internalization/dissociation of ^{125}I-IL-13

Cell Lines	κ_{in} (h^{-1})	κ'_{in} (h^{-1})	κ_1 (h^{-1})	κ_2 (h^{-1})	$z_f^0/(z_f^0 + z_s^0)$
HL	1.74	0.00	2.9	0.096	0.41
ML_{neo}	1.50	0.00	0.78	0.072	0.32
ML_γ	1.26	0.00	2.22	0.084	0.30

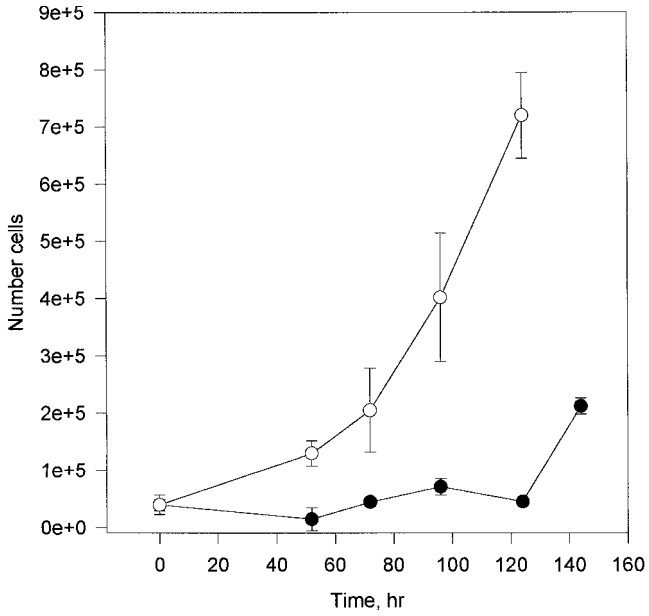

FIGURE 11 Effect of γ_c-transfection on kinetics of RCC growth. 35,000 ML_{neo} cells (—●—) or $ML\gamma_c$ cells (—○—) were cultured in duplicate Petri dishes for different periods of time as described in Material and Methods. The exponential model of cell growth fit to experimental data for ML_{neo} cells and $ML\gamma_c$ cells at doubling times $\tau = 64$ h, and $\tau = 30$ h, respectively.

We demonstrate that the kinetics of IL-13R binding on ML-RCC cells cannot be explained by a one-receptor model. A two-independent receptor model fit our data for $ML\gamma_c$-transfected cells (Fig. 6), but this model (and its modifications) did not fit for ML_{neo} RCC cells. Furthermore, we observed time-dependence of association rate constants for control ML_{neo} RCC cells. Binding, dissociation, and displacement experiments do not quantitatively follow common classical ligand-receptor models and were rejected with statistical goodness-of-fit analysis.

When we applied a one-receptor model, then the apparent rate of binding and the number of IL-13 binding sites depended upon the initial ligand concentration (Figs. 4 and 5). This phenomenon has not been reported previously for any interleukin receptors. Dependence of a binding rate constant on ligand concentration has been well established for molecular-surface interactions for several ligand-receptor systems (Franco et al., 1996; Sadana and Beelaram, 1996a,b). The high fractal dimension of control RCC cell surfaces in comparison with γ_c-transfected RCC cells is consistent with our light microscopic observations in that $ML\gamma_c$ cells exhibit some morphological differences. The $ML\gamma_c$ RCC cells appear about 65% smaller, more elongated, and smoother than the ML_{neo} RCC cells (data not shown). We estimated that the fractal dimension of the surface of control cells (ML_{neo}) is significantly higher ($D_f \approx 2.4$) than the fractal dimension of the surface of γ_c-transfected RCC cells ($D_f \approx 1.9$) (Fig. 3 *D*). Our estimation of the fractal dimension D_f for ML-RCC cells correlates with digital image analysis data of membrane profiles of other tumor cells that have shown morphological complexity and high fractal dimension (Keough et al., 1991; Nonnenmacher et al., 1994). Thus, the kinetic anomalies observed in our system may be explained by the effects of nonuniform distribution of receptor molecules in different domains of the cell surface. The cell surface complexity may provide more favorable physical conditions for accumulation of the receptor molecules on some domains and for receptor clusterization in these domains. In contrast, local complexity of the landscape of the cell surface may provide physical constrains for diffusion of IL-13 molecules and its interaction with the receptors in some surface domains. Based on fractal kinetic analysis, we assume that a small fraction of IL-13 receptor molecules pre-exists as microclusters (at least, as dimers) (Fig. 12). Because modulation effects of surface complexity on association rate of IL-13 appears to be a nonspecific for IL-13 binding, we predict that a similar cooperative effect in ligand binding may exist for other types of receptors expressed on ML_{neo} cells.

We have developed a stoichiometric model for IL-13 interaction with its receptors expressed on RCC cells. The conceptual schema of our model draws on Fig. 12. According to this model, the IL-13R$\alpha(\alpha_2)$ chain binds IL-13 with high affinity. Referred to the recent data (Donaldson et al., 1998; Puri et al., unpublished data), we proposed that high affinity IL-13 Rα alone may bind IL-13. Furthermore, ML-RCC cells express coreceptor molecules, which enhance the association rate binding of IL-13. This coreceptor molecule stabilizes ligand on the cell surface for a long period of time causing release of inhibitor molecule(s). Our model predicts the expression of a large number of the primary IL-13 receptors (360×10^3 copies per cell) and the coreceptor molecules (about 340×10^3 copies per cell) on the cell surface. The identify of this coreceptor molecule is not known. The IL-4 receptor β chain forms a complex with IL-13Rα', it is possible that the β chain works as a coreceptor molecule. However, expression of this chain on the cell surface of ML-RCC cells is more limited than is the IL-13α' chain (Caput et al., 1996; Obiri et al., 1996b). It is possible that the IL-13α' chain molecule is a candidate for a coreceptor in our model. IL-13Rα' chain alone binds IL-13 with a much lower affinity than does IL-13Rα (Murata et al., 1998), however, α' chain forms a high affinity IL-13R complex with IL-14β chain. Because the inhibitor-ligand complex is assumed to be unable to bind to primary receptors R_1 and R_2 (Fig. 12; R_1 is the IL-13α receptor and R_2 is the heterodimer IL-13α'–IL-4β), the IL-13 binding to the cell is self-regulated. Recently, the soluble form of the high-affinity IL-13 binding protein (IL-13BP) has been detected in the serum and urine of mice (Zhang et al., 1997). This protein binds IL-13 with a 100–300-fold higher affinity than does cloned IL-13Rα'. A soluble form of IL-13Rα' chain was also detected in the supernatant of activated peripheral blood T cells (Graber et al., 1998). These findings, together with predictions of our model, allow us to propose that, in human ML-RCC cells, IL-13 binding can induce shedding of a high-affinity soluble form(s) or frag-

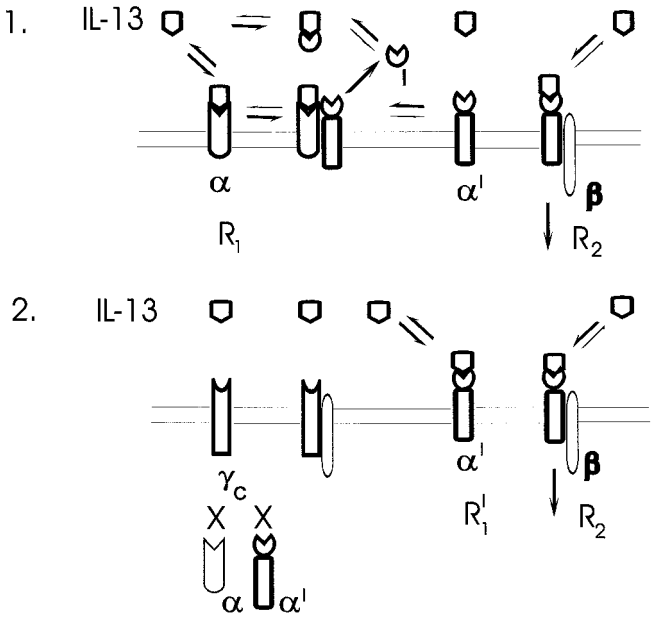

FIGURE 12 Proposed model for IL-13 interaction with its receptors on RCC cells (1) without and (2) with expression of IL-2 γ_c-chain. IL-13 has been shown to bind low-affinity and high-affinity ~70 kDa proteins termed IL-13R$\alpha_1(\alpha')$ and IL-13R$\alpha_2(\alpha)$, respectively. A relatively small fraction of IL-4 receptor β, but no γ_c-chain were also observed on RCC cells. IL-13R are naturally highly expressed on RCC cells. We assume that the vast majority of IL-13Rs express only a single binding site; the IL-4 receptor β chain forms dimer with α' chain. It is believed that the α'–β heterodimer pre-exist on the cell membrane of RCC cells before interaction with the IL-13 molecule, and the number of copies of this receptor complex depends on the level of morphological complexity (fractality) of the cell membrane. In the first model, IL-13 binds initially to high-affinity receptors α and α'–β, then the ligand–α-receptor complex interacts with the coreceptor molecule (α'). Binding IL-13 to α'–β heterodimer explains a positive cooperativity in kinetics of ^{125}I-IL-13 binding. Release of inhibitor molecule(s) (I) is mediated by the trimeric IL-13α–IL-13–α' complex. The extracellular domain of α' (and/or α) chain can be cleaved and shed. This domain can reduce further binding of IL-13 to membrane forms of IL-13Rs. Binding and dissociation processes, interconversion of complex states and internalization of ligand-receptor complex are shown by arrows. The thickness of the arrows schematically indicates the rate of the process. In the second model, expression of γ_c chain in cell prevents the expression of α chain molecules and partially reduces expression of α' chain. Symbol X implies inhibition of mRNA transcription of these proteins. Because γ_c forms a functional complex with IL-4Rβ chain and β chain has stronger affinity to γ_c than to IL-13Rα', β chain can rebind to γ_c, and the number of high-affinity binding sites for IL-13 will be reduced. Because only β chain has a long intracellular tail, we propose that only IL-13–α'–β complex can be internalized. Thus, both our models demonstrate that the internalization of ligand-receptor complex is mediated by fast and high-affinity α'–β receptor complex.

ment(s) of IL-13R, which should be an effective inhibitor of biological activities of IL-13. Further studies will examine these and other possibilities of self-regulatory mechanisms of activity of the IL-13R complex.

Our conceptual model of IL-13 binding to control cells (Fig. 12) was not rejected by a goodness-of-fit analysis (Figs. 7 and 8) and agreed with the literature. Moreover, this model provided an explanation of two-phase dissociation kinetics of ligand from the cell surface. Additionally, it demonstrates the independence of the bound fraction of IL-13 at the steady state from the initial concentration of IL-13. Furthermore, our model of IL-13 binding in γ_c-transfected cells predicted that during the early phase of IL-13 binding, intermediate-affinity binding sites were occupied, whereas, at the steady state, very high-affinity binding sites dominated (Fig. 6 *D*).

The decrease in IL-13 binding upon γ_c-transfection in ML-RCC cells, described here, agrees with our previous report (Obiri et al., 1996b). However, the molecular mechanism and the significance of this decrease in IL-13 binding is still not known. Because IL-13Rα mRNA was not detected in MLγ_c-transfected cells (Obiri et al., 1996b), it is reasonable to assume that γ_c-transfected cells did not express the IL-13α chain on the cell membrane. The expression of IL-13α' mRNA in MLγ_c cells was approximately three times less than that of control cells (Obiri et al., 1996b). Because genes encoding γ_c and IL-13Rα' are localized in the close region of the X chromosome, it is possible that the expression of γ_c gene suppresses the expression of IL-13Rα gene. These predictions are represented in our model in Fig. 12. According to this model, γ_c-transfected cells are shown to lack the IL-13Rα chain and have a dramatically decreased expression level of the IL-13Rα' chain.

The increase in the association rate of IL-13 binding correlates with expression of γ_c chain. The explanation for this is not clear, but may be related to a stabilizing effect of γ_c on the IL-13–IL-13R interaction. This effect is well documented for the IL-2R complex (Matsuoka et al., 1993; Chang et al., 1996; Borisova and Kuznetsov, 1996). It is possible that over-expression of γ_c masks the binding site of moderate affinity IL-13R by steric hinderance inhibiting IL-13 binding. It is also possible that the over-expression of γ_c-chain on cell membranes allosterically alters the conformation of the IL-13 receptor complex resulting in a decreased number of binding sites and affinity. Further studies are necessary to define the exact mechanism of these interactions.

This is the first report demonstrating IL-13 induced receptor-mediated internalization. We show that only 14–24% of the surface bound ligand-receptor complexes were rapidly internalized (within 15–40 min), and similar fractions are dissociated in both control and γ_c-transfected cells. The majority of radiolabeled receptor complex (60–70%) remained on the cell surface, and this was unchanged for up to 5 h of incubation. These data suggest that IL-13R exists in two different forms on RCC cells (or steady-state conformation states); one form is internalized and the other is noninternalized. These two forms of IL-13–IL13R complex are distinguishable on the cell surface for up to 40 min of ligand processing at 37°C.

Interestingly, expression of γ_c gene decreased the number of binding sites for IL-13, reduced the dissociation rate constants of IL-13R, and increased the association rate constants, but it did not modify the steady-state ratio between the amounts of internalized and noninternalized

forms of IL-13R. It also did not change the rate of receptor-mediated internalization of IL-13 (Fig. 10, Table 3). These data suggest that, in γ_c-transfected cells, the mechanism of receptor-mediated endocytosis of IL-13 remains intact. But γ_c transfection exerts a profound effect on the relationship between the different types of IL-13 receptor subunits and its binding activity. The structural and kinetic changes presented here correlate with changes in signal transduction pathways of IL-13 (Obiri et al., 1996a, 1997) and a faster proliferation of MLγ_c-transfected cells compared to control RCC cells.

In conclusion, we have demonstrated that, for the IL-13R system, the apparent rate of binding, but not dissociation, depends upon ligand concentration. These observations provide a basis for a new theoretical model for membrane organization of IL-13R and indicate that the traditional experimental design for the determination of receptor number and affinity of IL-13R needs to be carefully examined. We also demonstrated that IL-13 receptors are heterogeneous in binding and physiological processes. A fraction of IL-13R(s) is rapidly internalized after binding to the ligand, another fraction of bound receptor stays on the cell surface for many hours. These observations may help explain, at least in part, the very potent cytotoxic effect of IL-13 toxin on RCC cells that express IL-13R (Puri et al., 1996a) and the growth inhibitory effect of IL-13 at low concentration of IL-13 (Obiri et al. 1996a). Further analysis of these correlations should be developed based on the structure-kinetic approach presented here.

Dr. V. A. Kuznetsov's stay at the Laboratory of Molecular Tumor Biology was supported by a fellowship grant from the American Cancer Society, and International Union Against Cancer grant, and a Short-Term Scientist Exchange Program grant from the National Cancer Institute/NIH. We thank Dr. Gary D. Knott for very fruitful discussions of mathematical models and for the MLAB modeling program. We also thank Ms. Pamela Leland for excellent technical assistance, and Drs. Nicholas Obiri, S. Rafat Husain, Takashi Murata, Ralf Nossal, Zvi Grossman, and Peter Munson, for critical reading of this manuscript.

REFERENCES

Bajzer, Z., A. Myers, and S. Vuk-Pavlovic. 1989. Binding, internalization, and intracellular processing of proteins interacting with recycling receptors. *J. Biol. Chem.* 264:13623–13631.

Berg, H. C., and E. M. Pursell. 1977. Physics of chemoreception. *Biophys. J.* 20:193–219.

Borisova, L. R., and V. A. Kuznetsov. 1996. Structural-kinetics models of interaction of interleukin-2 (IL-2) with multi-subunit receptor and its internalization. *Chem. Phys. Rep.* 15:108–125.

Caput, D., P. Laurent, M. Kaghad, J.-M. Lelias, S. Lefort, N. Vita, and P. Ferrare. 1996. Cloning and Characterization of a specific interleukin (IL)-13 binding protein structurally related to the IL-5 receptor alpha chain. *J. Biol. Chem.* 271:16921–16926.

Chang, D. Z., Z. Wu, and T. L. Ciardelli. 1996. A point mutation in Interleukin-2 that alters ligand internalization. *J. Biol. Chem.* 271: 13349–13355.

Chaouchi, N., C. Wallon, C. Goujard, G. Tertain, A. Rudent, D. Caput, P. Ferara, A. Minty, A. Vazquez, and L.-F. Delfraissy. 1996. Interleukin-13 inhibits interleukin-2-induced proliferation and protects chronic lymphocytic leukemia B cells from in vitro apoptosis. *Blood.* 87:1022–1029.

Debinski, W., N. I. Obiri, I. Pastan, and R. K. Puri. 1995. A novel chimeric protein composed of interleukin 13 and *Pseudomonas* exotoxin is highly cytotoxic to human carcinoma cell expressing receptors for interleukin 4. *J. Biol. Chem.* 270:16775–16780.

Donaldson, D. D., M. J. Whitters, L. J. Fitz, T. Y. Neben, H. Fimnnerty, S. L. Henderson, R. M. O'Harra, D. R. Beair, K. J. Turner, C. R. Wood, and M. Collings. 1998. The murine IL-13 receptor alpha 2: molecular cloning, characterization, and comparison with murine IG-13 receptor alpha 1. *J. Immunol.* 161:2317–2724.

Erickson, J., B. Goldstein, D. Holowka, and B. Baird. 1987. The effect of receptor density on the forward rate constant for binding of ligand to cell surface receptors. *Biophys. J.* 52:657–662.

Franco, R., V. Casado, F. Ciruela, J. Mallol, C. Lluis, and E. I. Canela. 1996. The cluster-aggregated cooperative model: a model that accounts for the kinetics of binding to A_1 adenosine receptors. *Biochemistry.* 35:3007–3015.

Gex-Fabry, M., and C. DeLisi. 1984. Receptor-mediated endocytosis: a model and its implication for experimental analysis. *Am. J. Physiol.* 247:R768–R779.

Goldstein, B., and M. Dembo. 1995. Approximating the effect of diffusion on reversible reactions at the cell surface: ligand-receptor kinetics. *Biophys. J.* 68:1222–1230.

Goldstein, B., D. Jones, I. G. Kevrekidis, and A. S. Perelson. 1992. Evidence for p55–p75 heterodimers in the absence of IL-2 from Scatchard plot analysis. *Intern. Immunol.* 4:23–32.

Goldstein, B., R. G. Posner, D. C. Torney, J. Erickson, D. Holowka, and B. Baird. 1989. Competition between solution and cell surface receptors for ligand: the dissociation of hapten bound presence of surface antibody in the presence of solution antibody. *Biophys. J.* 58:955–966.

Graber, P., D. Gretener, S. Herren, J. P. Aubry, G. Elson, J. Poudrier, S. Lecoanet-Henchoz, S. Alouani, C. Lisberger, J. Y. Bonnefoy, M. H. Kosco-Vilbois, and J. F. Gauchat. 1998. The distribution of IL-13 receptor alpha 1 expression on B cells, T cells and monocytes and its regulation by IL-113 and IL-4. *Eur. J. Immunol.* 28:4226–4298.

Havlin, S. 1989. Molecular diffusion and reactions. *In* The Fractal Approach to Heterogeneous Chemistry: Surfaces, Colloids, Polymers. D. Avnir, editor. Wiley and Sons Ltd., New York, NY. 251–269.

Keough, K. M. W., P. Hyam, D. A. Pink, and B. Quinn. 1991. Cell surfaces and fractal dimensions. *J. Micro.* 163:95–99.

Knott, G. 1996. MLAB: A mathematical modeling laboratory. Civilized Software, Bethesda, MD.

Kuznetsov, V. A. 1990. Computer analysis of receptor-mediated endocytosis and exocytosis mechanisms: two pathways for the progressing of Ti/CD3 receptor complexes of T lymphocytes. *Biomed. Sci.* 1:631–638.

Kuznetsov, V. A. 1996. Basic models of tumor-immune system interactions: identification, analysis and predictions. *In* A Survey of Models for Tumor-Immune System Dynamics. J. A. Adam and N. Bellomo, editors. Birkhauser, Boston, MA. 237–290.

Kuznetsov, V. A., and L. P. Borisova. 1995a. Kinetics model of the interleukin-4 (IL-4) binding to high affinity IL-4 receptor and their internalization. *In* Differential Equations and Applications to Biology and to Industry. M. Martelli, K. Cooke, E. Cumberbatch, B. Tang, H. Thieme, editors. Word Science Publishing Co., Singapore–N.Y.–London–Hong Kong–Bangalore. 271–280.

Kuznetsov, V. A., and L. R. Borisova. 1995b. Kinetic analysis of the internalization and shedding of interleukin-2 from surface of cells expressing receptors of different affinity. *Membr. and Cell Biol.* 8:591–604.

Kuznetsov, V. A., V. P. Zhivoglyadov, and L. A. Stepanova. 1993. Kinetic approach and estimation of parameters of cellular interaction between immunity system and a tumor. *Arch. Immunol. Ther. Exp.* 41:21–31.

Matsuoka, M., T. Takeshita, N. Ishii, M. Nakamura, T. Ohkubo, and K. Sugamura. 1993. Kinetic study of interleukin-2 binding on the reconstituted interleukin-2 receptor complex including the human γ chain. *Eur. J. Immunol.* 23:2472–2476.

McKenzie, A. N. J., J. A. Culpepper, R. de Waal Malefyt, F. Briere, J. Punnonen, G. Aversa, A. Sato, W. Dang, B. G. Cocks, S. Menon, J. E. de Vries, J. Blanchereau, and G. Zurawski. 1993. Interleukin-13, a T cell-derived cytokine that regulate human monocyte and B cell function. *Proc. Natl. Acad. Sci. USA.* 90:3735–3739.

Minty, A., P. Chalon, J.-M. Derocq, X. Dumount, J.-C. Gullemot, M. Kaghad, C. Labit, P. Leplatois, P. Laiauzun, B. Miloux, C. Minty, P. Casellas, G. Loison, J. Lupker, D. Shire, P. Ferrara, and D. Caput. 1993. Interleukin-13 is a new lymphokine regulating inflammatory and immune responses. *Nature.* 362:248–250.

Murata, T., N. Obiri, W. Debinski, and R. K. Puri. 1998. Structure of IL-13 receptor: analysis of subunit composition in cancer and immune cells. *Biochem. Biophys. Res. Comm.* 238:90–94.

Nonnenmacher, T. F., G. Baumann, A. Barth, and G. A. Losa. 1994. Digital image analysis of self-similar cell profiles. *Int. J. Biomed. Computing.* 37:131–138.

Obiri, N. I., W. Debinski, W. J. Leonard, and R. K. Puri. 1995. Receptor for interleukin 13. Interaction with interleukin 4 by a mechanism that does not involve the common γ chain shred by receptors for interleukins 2, 4, 7, 9 and 15. *J. Biol. Chem.* 270:8797–8804.

Obiri, N. I., G. Hillman, G. P. Haas, S. Sudha, and R. K. Puri. 1993. Expression of high affinity Interleukin-4 receptors on human renal carcinoma cells and inhibition of tumor growth in vitro by Interleukin-4. *J. Clin. Invest.* 91:88–93.

Obiri, N. I., S. R. Husain, W. Debinski, and R. K. Puri. 1996a. Interleukin 13 inhibits growth of human renal cell carcinoma cells independently of the p140 interleukin 4 receptor chain. *Clin. Cancer Res.* 2:1743–1749.

Obiri, N. I., T. Murata, W. Debinski, and R. K. Puri. 1997. Modulation of interleukin-13 binding and signalling by the γ_c chain of the IL-2 receptor. *J. Biol. Chem.* 272:20251–20258.

Obiri, N. I., P. Leland, T. Murata, W. Debinski, and R. K. Puri. 1997. The IL-13 receptor structure differs on various cell types and may share more than one component with IL-4 receptor. *J. Immunol.* 158:756–764.

Obiri, N. I., and R. K. Puri. 1994. Characterization of IL-4 receptor expressed on human renal carcinoma cells. *Oncol. Res.* 6:419–427.

Park, L. S., D. Friend, H. M. Sassenfield, and D. L. Urdal. 1987. Characterization of the human B cell stimulatory factor 1 receptor. *J. Exp. Med.* 166:476–488.

Posner, R. G., B. Lee, D. H. Conrad, D. Holowka, B. Baird, and B. Goldstein. 1992. Aggregation of IgE-receptor complex on rat basophilic leukemia cells does not change the intrinsic affinity but can alter the kinetics of the ligand-IgE interaction. *Biochemistry.* 31:5350–5356.

Puri, R. K., N. I. Obiri, S. R. Husain, R. J. Kreitman, G. P. Haas, I. Pastan, and W. Debinski. 1996a. Targering of interleukin 13 receptors on human renal cell carcinoma cells by a recombinant chimeric protein composed of interleukin-13 and trucated form of *Pseudomonas* exotoxin A (PE38QQ8). *Blood.* 87:4333–4339.

Puri, R. K., P. Leonard, N. I. Obiri, S. R. Husain, J. Mule, I. Pastan, and R. J. Kreitman. 1996b. An improved circulatory permited interleukin 4-toxin is highly cytotoxic to human renal cell carcinoma cells. Introduction of γ_c chain in RCC cells does not improve sensitivity. *Cell. Immunol.* 171:80–86.

Rovati, G. E., R. Shrager, S. Nicosia, and P. J. Munson. 1996. KINET II: a nonlinear least-squares program for analysis of kinetic binding data. *Mol. Pharmacol.* 50:86–95.

Sadana, A., and A. M. Beelaram. 1996a. Antigen-antibody diffusion-limited binding kinetics for biosensors. A fractal analysis. *Appl. Biochem. Biotech.* 59:259–282.

Sadana, A., and A. M. Beelaram. 1996b. Antigen-antibody binding kinetics for biosensors: changes in fractal dimension (surface roughness) and in the binding rate coefficient. *Appl. Biochem. Biotech.* 60:123–1138.

de Waal Malefyt, R., C. G. Figdor, R. Hui Jbens, S. Mohan-Peterson, B. Bennett, J. Culpepper, W. Dang, G. Zurawski, and J. E. de Vries. 1993. Effects of IL-13 on phenotype, cytokine production, and cytotoxic function of human monocytes. Comparision with IL-4 and modulation by IFN-γ or IL-10. *J. Immunol.* 150:6370–6376.

Wofsy, C., B. Goldstein, K. Lung, and H. S. Willey. 1992. Implications of epidermal growth factor (EGF) induced EGF receptor aggregation. *Biophys. J.* 63:98–110.

Zhang, J. G., D. J. Hilton, T. A. Willson, C. McFarlane, B. A. Roberts, R. L. Moritz, R. J. Simpson, W. S. Alexamder, D. Metcalf, and N. A. Nicola. 1997. Identification, purification, and characterization of a soluble Interleukin (IL)-13-binding protein. *J. Biol. Chem.* 282:9474–9480.

Zurawski, G., and J. E. de Vries. 1994. Interleukin-13 and Interleukin-4-like cytokine that acts on monocytes and B cells but not on T cells. *Immunol. Today.* 15:19–26.